NASA/CR—1999-209160

Forced Mixer Nozzle Optimization

Yogi Sheoran, Robert Hoover, William Schuster, Morris Anderson, and
Donald S. Weir
AlliedSignal Engines, Phoenix, Arizona

September 1999

The NASA STI Program Office . . . in Profile

Since its founding, NASA has been dedicated to the advancement of aeronautics and space science. The NASA Scientific and Technical Information (STI) Program Office plays a key part in helping NASA maintain this important role.

The NASA STI Program Office is operated by Langley Research Center, the Lead Center for NASA's scientific and technical information. The NASA STI Program Office provides access to the NASA STI Database, the largest collection of aeronautical and space science STI in the world. The Program Office is also NASA's institutional mechanism for disseminating the results of its research and development activities. These results are published by NASA in the NASA STI Report Series, which includes the following report types:

- TECHNICAL PUBLICATION. Reports of completed research or a major significant phase of research that present the results of NASA programs and include extensive data or theoretical analysis. Includes compilations of significant scientific and technical data and information deemed to be of continuing reference value. NASA's counterpart of peer-reviewed formal professional papers but has less stringent limitations on manuscript length and extent of graphic presentations.

- TECHNICAL MEMORANDUM. Scientific and technical findings that are preliminary or of specialized interest, e.g., quick release reports, working papers, and bibliographies that contain minimal annotation. Does not contain extensive analysis.

- CONTRACTOR REPORT. Scientific and technical findings by NASA-sponsored contractors and grantees.

- CONFERENCE PUBLICATION. Collected papers from scientific and technical conferences, symposia, seminars, or other meetings sponsored or cosponsored by NASA.

- SPECIAL PUBLICATION. Scientific, technical, or historical information from NASA programs, projects, and missions, often concerned with subjects having substantial public interest.

- TECHNICAL TRANSLATION. English-language translations of foreign scientific and technical material pertinent to NASA's mission.

Specialized services that complement the STI Program Office's diverse offerings include creating custom thesauri, building customized data bases, organizing and publishing research results . . . even providing videos.

For more information about the NASA STI Program Office, see the following:

- Access the NASA STI Program Home Page at ***http://www.sti.nasa.gov***

- E-mail your question via the Internet to help@sti.nasa.gov

- Fax your question to the NASA Access Help Desk at (301) 621-0134

- Telephone the NASA Access Help Desk at (301) 621-0390

- Write to:
  NASA Access Help Desk
  NASA Center for AeroSpace Information
  7121 Standard Drive
  Hanover, MD 21076

NASA/CR—1999-209160

Forced Mixer Nozzle Optimization

Yogi Sheoran, Robert Hoover, William Schuster, Morris Anderson, and
Donald S. Weir
AlliedSignal Engines, Phoenix, Arizona

Prepared under Contract NAS3–27483, Task Order 7

National Aeronautics and
Space Administration

Glenn Research Center

September 1999

Available from

NASA Center for Aerospace Information
7121 Standard Drive
Hanover, MD 21076
Price Code: A04

National Technical Information Service
5285 Port Royal Road
Springfield, VA 22100
Price Code: A04

Table of Contents

1.0 INTRODUCTION

The primary objective of the forced mixer optimization program is to design an advanced mixer nozzle system (AMNS) for 3 to 6 bypass ratio engines to achieve a 3 EPNdB reduction of the jet exhaust noise relative to the baseline nozzle system.

Computational fluid dynamic (CFD) and computational acoustic analyses were performed for the TFE731-60 (originally TFE731-5A) mixer nozzle and an E^3 mixer nozzle for comparison with available data. Initial aerodynamic designs of three new nozzle systems were performed to determine the configuration with the best aerodynamic and acoustic performance. Based on the initial results, a new nozzle system was designed that includes the best features identified during the initial studies, and the aerodynamic and acoustic performance was predicted.

2.0 BACKGROUND

Nozzle design and optimization is a key part of the AlliedSignal Engine (AE) development process. AE has developed extensive expertise in the design, development, and testing of mixer nozzles during the past 20 years. During this time period, AE has designed numerous mixer nozzle systems, including the Quite and Clean General Aviation Turbofan (QCGAT) mixer nozzle, the TFE731-3 and the TFE731-5A/B production mixer nozzle, and several others for special applications.

QCGAT. The objective of the NASA Quiet and Clean General Aviation Turbofan program was to demonstrate that large turbofan design concepts can be successfully applied to turbofan engines with general aviation applications. Regional transports share many performance and cost goals with the general aviation community. The program goals were to improve the environmental characteristics of civil aircraft by reducing noise and pollution near airports, thereby assisting in reducing growth restraints to civil aviation, and also providing engines with reduced fuel consumption.

During the QCGAT program, AE laid the foundation for its mixer nozzle design and development procedure. A preliminary mixer geometry optimization computer code (MIX) was developed and used to perform parametric studies of mixer geometric effects on overall performance. The mixer lobe designs were analyzed with a 3-D viscous compressible flow code. The configurations were also analyzed for mixing efficiency, using the parabolic turbulent mixing-model code, PARMIX. Based on the results of the analysis, candidate mixer configurations were selected for scale-model testing. Hardware was fabricated and rig tested. Rig testing was conducted at FluiDyne. Performance and acoustic data were recorded at sea-level static takeoff and cruise design point conditions. A final mixer exhaust system was selected and the scale-

scale-model was tested at off-design conditions to generate the performance maps. The performance maps were used in an engine cycle sizing analysis to obtain the optimum areas for the overall flight regime.

Six alternative geometries were analyzed to reduce loss and improve velocity distribution. The effects of lobe shape on the mixing process were assessed by studying the calculated total temperature, total pressure, and velocity profiles at the mixing duct exit plane. The final configuration was designed to full scale and hardware fabricated. Full-scale mixer hardware was tested on the QCGAT engine at NASA-Lewis in 1981. The QCGAT program goals were exceeded with cruise thrust specific fuel consumption (TSFC) reduction of 3.2 percent, and a sea-level static takeoff turbine inlet temperature reduction of 21.1F. Acoustic measurements were also made of the six QCGAT mixer configurations during testing at FluiDyne.

TFE731-5. The design process developed for QCGAT was successfully applied to design and develop the TFE731-5A mixer nozzle system, which was introduced into production in the middle 1980s, and is still being produced today for the TFE731-5B and TFE731-60.

The TFE731-5A mixer nozzle was recently analyzed using the commercially available FLUENT CFD code. A 3-D pie sector bounded by two symmetric boundaries extending circumferentially from the tip of the lobe to the valley was analyzed. FLUENT uses structured body-fitted nonadaptive grids. The 3-D viscous compressible turbulent flow analysis was a great improvement over the past approach of running three separate analysis in sequence to model the entire mixer nozzle system region. However because of computation time and memory limitations imposed by the use of structured grids the far field was not modeled.

CFE738. AE has contributed to the development and introduction into production of the CFE738 exhaust mixer nozzle system. Mechanical analysis was conducted on the mixer to help reduce weight and to produce a mixer nozzle manufactured for reliability and maintainability.

APU mixer eductors. AE has developed an oil-cooling exhaust eductor system by introducing the mixer nozzle to enhance the exhaust eductor performance. The oil-cooling exhaust eductor system was developed to eliminate the highly unreliable mechanically driven cooling fan system. The mixer nozzle was used to increase pumping capacity over the conventional eductor without incurring increased backpressure to the engine. The mixer nozzle also provided a quieter exhaust system. AE's 331-500 auxiliary power unit (APU) has completed its certification an oil-cooling exhaust eductor system. This technology has also been used in the 331-200UJ UNIJASU Navy's next-generation ground starting cart.

3.0 RESEARCH AND DESIGN

3.1 MGB Code Implementation

The improved MGB code, which calculates the jet mixing noise and shock noise for axisymmetric nozzles, was received from NASA Lewis and installed on the AlliedSignal computer system. The program requires the flow field data from a CFD analysis. In the current program, the PARC CFD code was used on a structured grid to generate the flow data. As a first step, the improved MGB code was run on a sample nozzle (see Reference 1) using the structured grid and the CFD results from the PARC program. The results of the comparison with the test case output file show that the program was transferred correctly.

A RAMPANT CFD model was created using geometry and boundary conditions specified by Khavaran, Krejsa and Kim. The nozzle (Figure 1) is an axisymmetric convergent-divergent nozzle operating at the following operating conditions.

- Nozzle Stagnation Pressure 42.227 psia
- Nozzle Stagnation Temperature 1716 °R
- Ambient Pressure 13.53 psia
- Ambient Temperature 540 °R
- Free Stream Velocity 400 fps
- Nozzle Area Ratio 1.119
- Throat Diameter 5.1 in

The plume was modeled 33+ exit diameters downstream of the nozzle exit as was done in Khavaran, Krejsa and Kim. The RAMPANT mesh contains about 23 000 fluid cells and was modified by adapting on gradients of static pressure, to get improved plume and shock definition, and wall nondimensional boundary layer parameter (y^+), to get improved wall boundary layer definition ($y^+<300$). The farfield size for the RAMPANT CFD runs are slightly larger than the base Khavaran farfield evaluated in NASA PARC. The boundary conditions for the RAMPANT model are a pressure inlet boundary for the nozzle inlet flow, a pressure farfield boundary for the left and upper farfield boundary and a pressure outlet for the right farfield boundary.

The initial mesh was created using the specification for an internal nozzle aerodynamic evaluation where the mesh was adapted to wall y^+ and gradients of static pressure. Further examination of the mesh near the nozzle exit (Figure 1b) shows good mesh detail on the nozzle internal flowfield where a shock pattern in present, and along the nozzle wall where good boundary layer definition is needed. However, in the plume/farfield shear layer immediately aft of the nozzle, mesh definition is relatively sparse compared to the PARC evaluation. When an MGB jet noise evaluation was run,

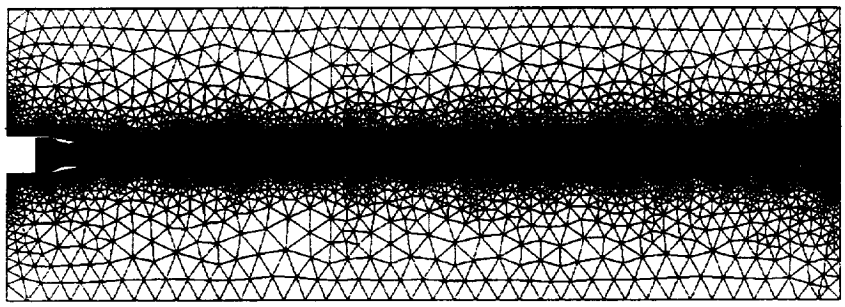

(a) Initial RAMPANT performance mesh

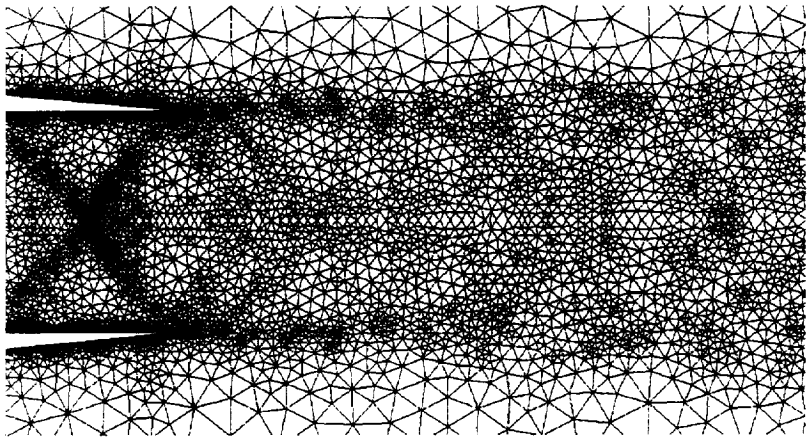

(b) Initial RAMPANT performance mesh - closeup of nozzle exit

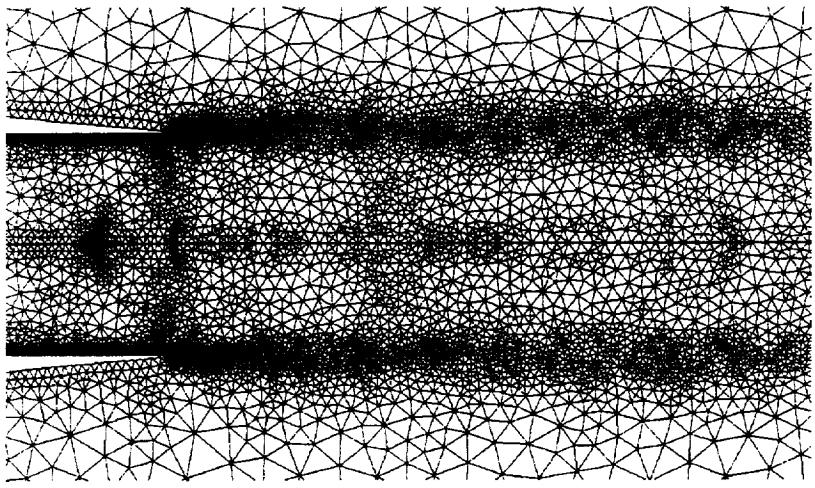

(c) Final RAMPANT mesh - adapted to gradients of Reynold's stress and dU/dy

Figure 1. A Computational Mesh Was Developed that Is Suitable for Acoustic Calculations.

the MGB results showed the RAMPANT CFD evaluation produced a similar sound power level (PWL) versus frequency shape, but at a lower PWL, particularly at high frequencies.

It was believed that this difference in PWL was due to inadequate mesh definition in the plume where the magnitude of turbulent kinetic energy (TKE) was greatest, so adaptations to gradients of TKE were made to the mesh. The adaptation increased mesh definition mid plume along the shear layer, however, little adaptation occurred near the nozzle exit. The model was rerun in RAMPANT and the RAMPANT results were evaluated in MGB. The MGB results showed an increase of low-frequency PWL to a greater level than obtained from the PARC analysis, however, at high frequencies, the PWL fell significantly below the levels from Khavaran's PARC analysis. These results indicated that the previous RAMPANT runs were not refined properly in the nozzle exit shear layer where shear layer is thinnest and the majority of the high-frequency noise is generated. A general rectangular region adaptation was completed on this region. A RAMPANT CFD evaluation was run on this mesh and its results were then evaluated in MGB. The results exhibited nearly the same PWL at low frequency, but the higher frequency noise was much higher. Unfortunately, this mesh required 47 000 fluid cells, indicating an inefficient use of fluid cells to complete the CFD solution. This leads to mesh size difficulties in using this meshing procedure in a 3-D model.

It was determined that adapting to gradients of fluid shearing, dU/dy for this plume, would automatically adapt the mesh in the correct areas to capture the TKE which generates the high-frequency noise. Adaptation to Reynolds stress (product of the turbulent viscosity and the shear derivative, dU/dy) was used to adapt the mesh further in the plume. The adapted mesh is shown in Figure 1c and contains 23 000 fluid cells. The nozzle and plume system Mach number contours are shown in Figure 2. Thus this method of adapting a coarse mesh in 2-D and 3-D was used in all other CFD models where jet noise was evaluated.

The MGB code only accepts structured grid flowfield information. Since the RAMPANT CFD program works with unstructured grids, it was decided to develop an interface to map the flowfield results from the unstructured RAMPANT grid to a structured PARC-style grid. To interface the flowfield results to the MGB code, a RAMPANT "journal file" was designed and coded which interpolates the unstructured grid results to the original PARC grid for the MGB test case. The grid geometry and flowfield data for the Khavaran test case were available as PLOT3D compatible files that were supplied with the jet noise program as shown in Figure 3.

The flow variables used by Khavaran's code are nondimensionalized values of density, x-momentum, y-momentum, total energy (extensive), TKE, and turbulent

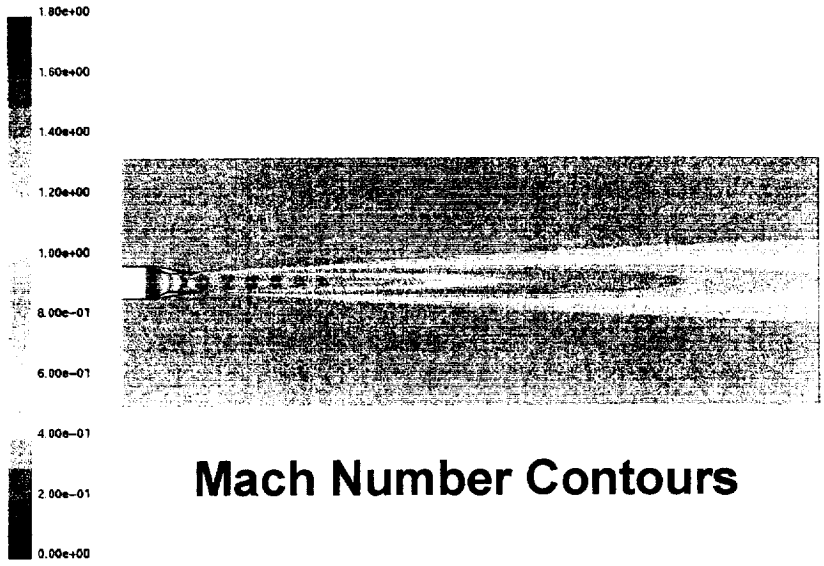

Figure 2. A Successful RAMPANT Flowfield Calculation Has Been Made for the Khavaran, Krejsa, and Kim Test Case.

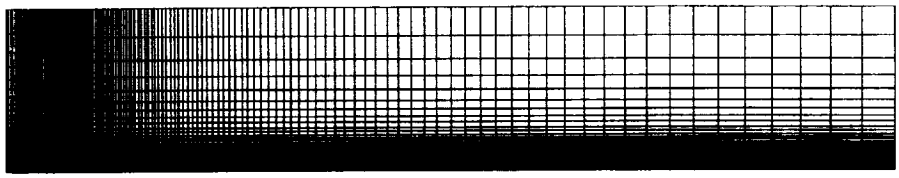

(a) overall view

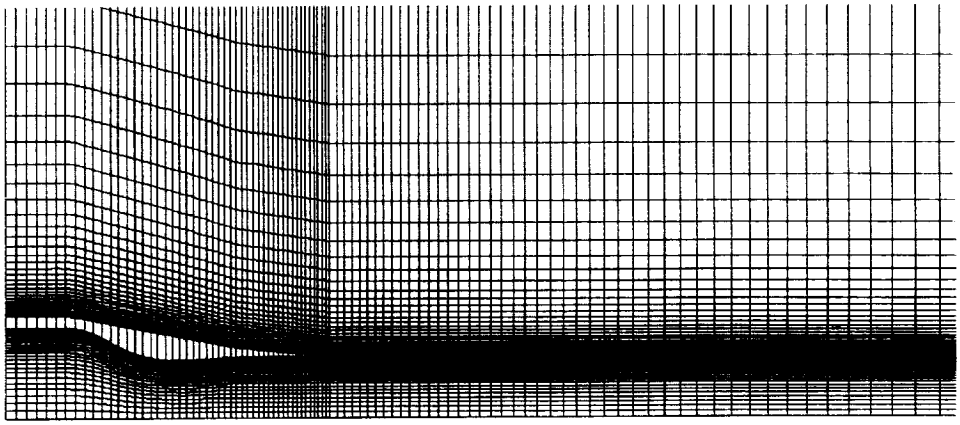

(b) Closeup of nozzle

Figure 3. Closeup of the PARC Mesh Shows Areas of Greatest Mesh Density.

dissipation rate ε. The TKE is a critical variable in the jet noise prediction program. If the levels of TKE in the narrow shear layer just downstream of the nozzle exit are underpredicted, then the high frequency noise generated by the turbulence in that region will also be underpredicted.

The structured PARC mesh is an orthogonal mesh consisting of 8601 points, 141 in the axial direction and 61 in the radial direction. The mesh density is greatest along the nozzle exit line in the axial direction and at the jet exit plane in the radial direction (see Figure 3). Only flowfield data in the jet plume is used in the noise generating noise predictions. The mesh extends 29.4 jet diameters in the downstream direction to capture the main body of turbulence responsible for the mixing noise. The unstructured mesh used in the RAMPANT analysis has the same overall dimensions.

Figure 4 contains a number of plots which compare flowfield data (density, TKE, x-momentum, ε , and total energy) for the PARC and interpolated RAMPANT data sets. Figure 5 contains comparisons of the corresponding jet noise predictions. There are some noticeable differences between the two data sets. For example, because the RAMPANT solution was generated on a much finer grid, the oscillatory (shock cell related) nature of some flow variables was more defined in the region inside and just aft of the nozzle than it was for the PARC data. Other differences between the two solution sets may be due to different methods in generating solutions (i.e., implementation of the k-ε model) and grid size effects.

3.2 Baseline nozzle

The TFE731-40 engine reference nozzle serves as the baseline for the AMNS design. The TFE731-40 engine received FAA certification on July 13, 1995. An extensive noise data base exists for the nozzle obtained during full scale engine testing. The following table summarizes the nozzle characteristics:

Configuration	Compound nozzle with convergent/divergent exit
Takeoff Bypass Ratio	3.48
Primary jet Velocity	1600 ft/sec
Primary Jet Temperature	1120F
Secondary Jet Velocity	920 ft/sec
Secondary Jet Total Temperature	160F

Acoustic test description. The AE acoustic test arena is located at the San Tan test site located southeast of Phoenix, Arizona. It is at an elevation of 1395 feet above sea level at the test stand and is a flat desert area free of any structures or other

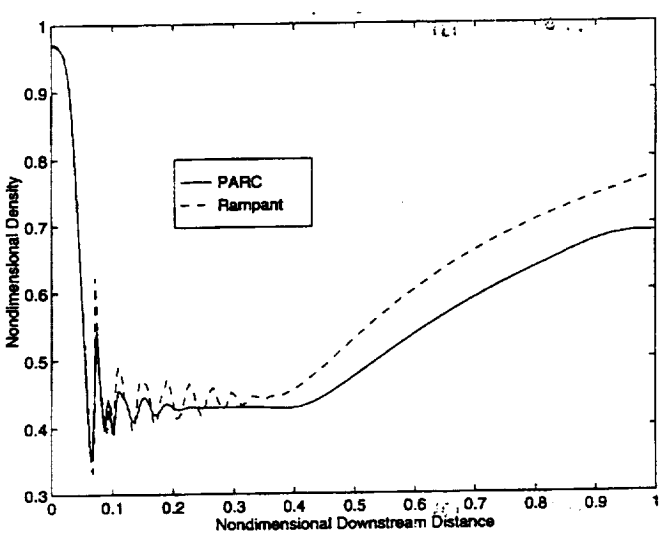

(a) centerline density

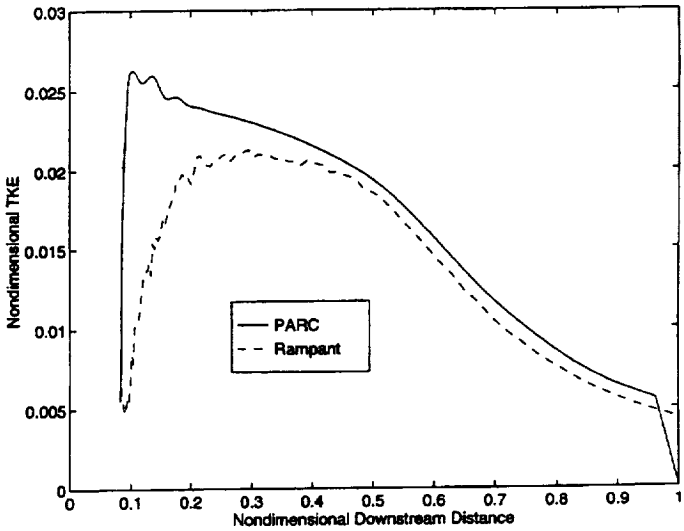

(b) nozzle exit line TKE

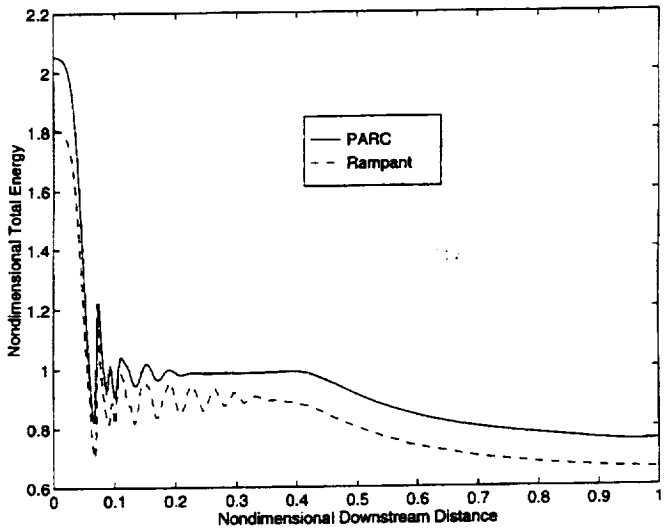

(c) centerline total energy

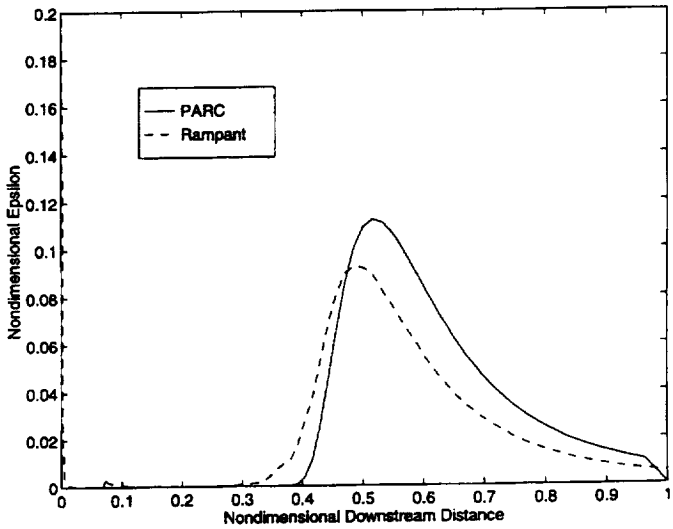

(d) centerline dissipation ε

Figure 4. Flow Variables Computed by RAMPANT and PARC Agree Well.

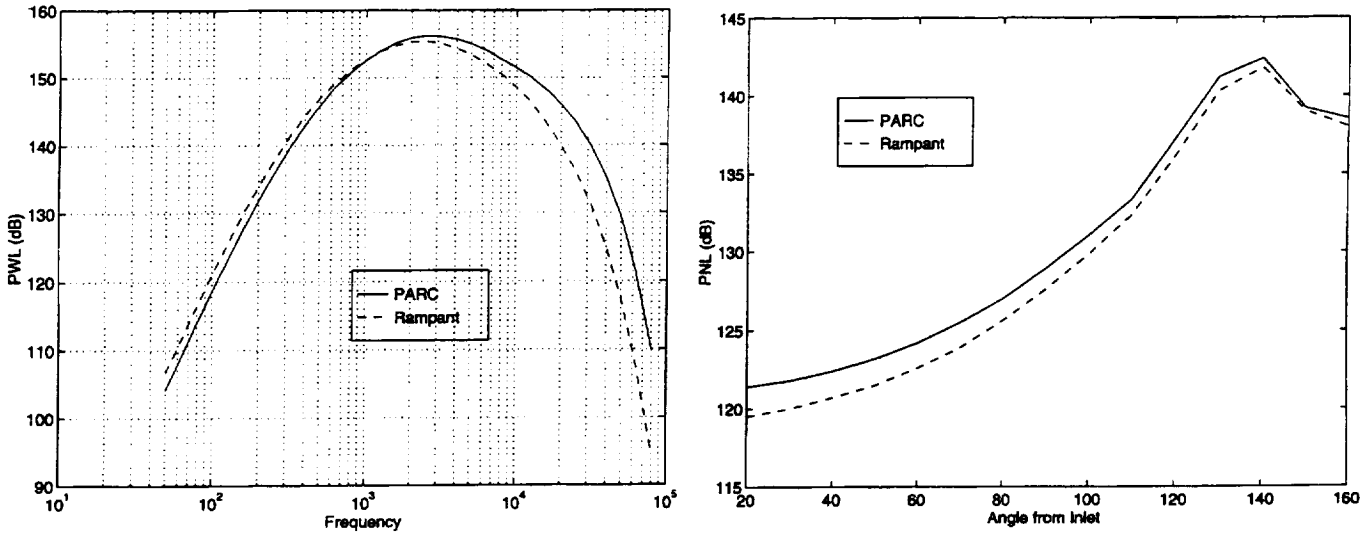

(a) overall power level (b) perceived noise level

Figure 5. The RAMPANT/MGB Interface Was Verified Using the MGB Supersonic Nozzle Test Case.

obstacles on the acoustic test arena. Since it is located at a remote site, the acoustic test arena has very low ambient noise levels.

The engine support structure for the acoustic test facility is of J-stand design to minimize the interference effects with both the acoustic propagation paths and the engine flowfield. A photograph of the stand is shown in Figure 6. The support for the stand is located on one side of the engine away from the microphone positions and is not in the direct propagation path. The support is also well out of the way of the engine inlet and exhaust to eliminate inflow distortion or exhaust impingement effects.

The engine is mounted on the stand such that the engine centerline is 10 feet above the ground. At this engine centerline height and with the use of the Inflow Control Device (ICD), there are no inflow distortion or exhaust impingement effects caused by the ground.

The Acoustic Test Facility was designed to meet all of the standards of SAE ARP 1846 (Reference 2). A schematic diagram of the facility is presented in Figure 7. The acoustic arena extends from beneath the engine to a distance that is at least 3 meters beyond all microphones. The engine support structure sits on a 58 by 58 ft. concrete pad. The concrete is uniformly smooth and hard, troweled level, and is light in color to minimize thermal gradients. The pad is surrounded by asphalt sloping downward at a 0.5 percent slope to allow for proper drainage. The asphalt is hard packed and uniform in texture. It is well sealed and painted white to minimize thermal gradients. Thus, the

entire acoustic arena surface is a near perfect sound reflector with no structures or natural obstacles. The engine fuel lines, control wiring, and microphone cables are run through underground conduits to prevent acoustic interference. The control room is located outside of the test arena at a distance of over 200 feet from the test stand on the opposite side from the microphones.

Figure 6. Photograph of an Engine at the San Tan Acoustic Test Facility Shows the Test Configuration.

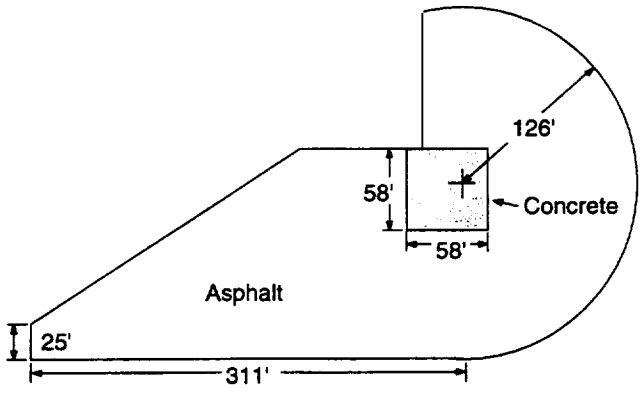

Figure 7. Layout of San Tan Acoustic Test Facility Shows Suitability for 100 ft. Polar Arc Acoustic Data.

Flowfield analysis. A RAMPANT analysis of the nozzle flowfield was performed at two performance cycle points, static take-off and cutback power points. These points are matched to test points for the TFE731-40 engine where acoustic data exists from the Acoustic Test Facility. The RAMPANT mesh created was generated using the guidelines needed to get proper acoustic results:

- Plume length to nozzle exit diameter equal to 25.
- Farfield height to nozzle exit radius greater than 10.

The final RAMPANT meshes for both models contain approximately 29 000 fluid cells and were adapted to wall y^+, static pressure, dU/dy, and Reynolds stress. Figure 8 shows the Reynold's stress contours for the sideline power point.

The RAMPANT analysis of the flowfield has been used to predict the noise using the MGB code and the results were compared to experimental data. The procedure for scaling the MGB structured grid to the TFE731-40 geometry has been established. The jet plume data were interpolated onto a structured mesh containing nearly 21 000 node points to form the input to the MGB jet noise code. The structured mesh was heavily refined in the axial direction near the nozzle exit and in the radial direction just outside the nozzle exit plane. Figure 9 summarize the sound power results for the full power and cutback thrust conditions respectively. Figure 10 shows several sound pressure level comparisons at directivity angles from the inlet of 80, 120, and 160 degrees.

The MGB noise results were compared to full engine acoustic test data. The overall noise levels compared reasonably well (within 2 to 5 dB) for frequencies up to 1000 Hz. The MGB results tended to overpredict noise levels. The MGB frequency spectra correlated well with test data frequency spectra for angles beyond 140 degrees. For lesser angles, MGB generally overpredicts noise levels (up to 10 dB). Modifying the MGB default parameter values to more closely model this moderate Mach number bypass flow brings the prediction into better correlation with the data. Use of the BETAMC parameter in the MGB code improved the comparison of the predicted acoustic power with the measured engine data.

3.3 Mixer Nozzle Modeling

The TFE731-60 mixer nozzle is a cutback 14-lobe TFE731-5A mixer. The only differences in the nozzles are area changes to accommodate the higher thrust level of the -60 and a change in the exit convergent/divergent nozzle design.

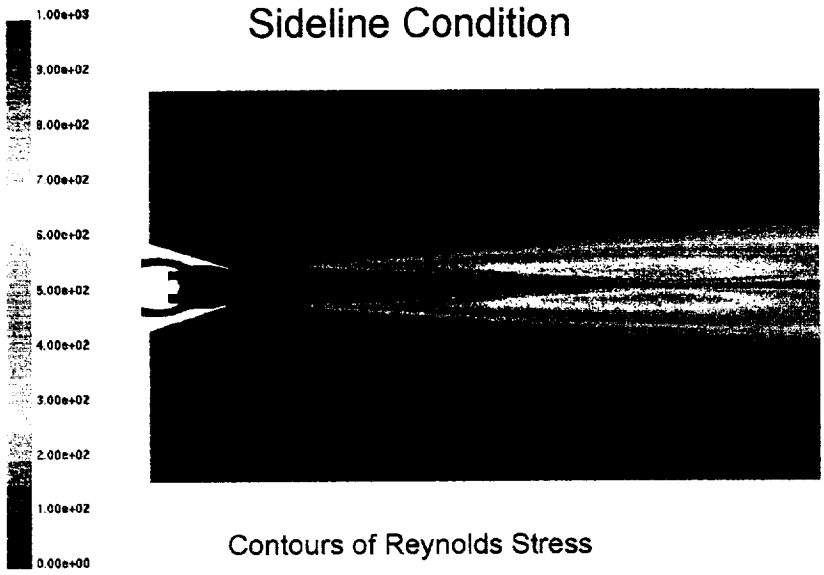

Figure 8. Successful RAMPANT Flowfield Calculations Have Been Made for the TFE731-40 Baseline Nozzle.

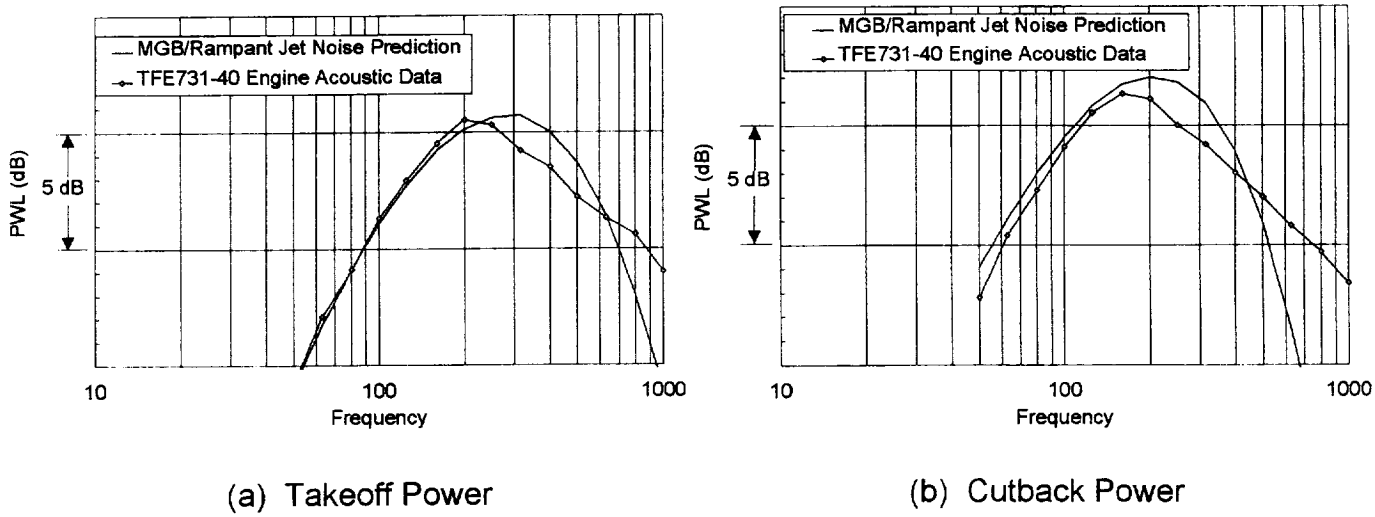

Figure 9. Successful MGB Sound Power Level Calculations Have Been Made for the TFE731-40 Baseline Nozzle.

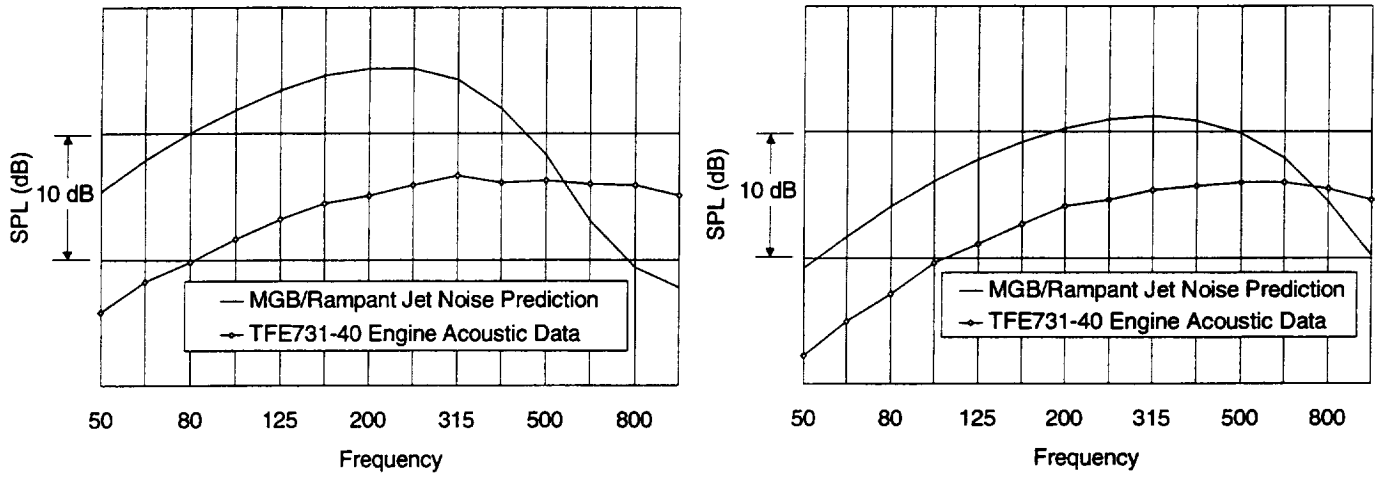

(a) 80 degrees from inlet

(b) 120 degrees from inlet

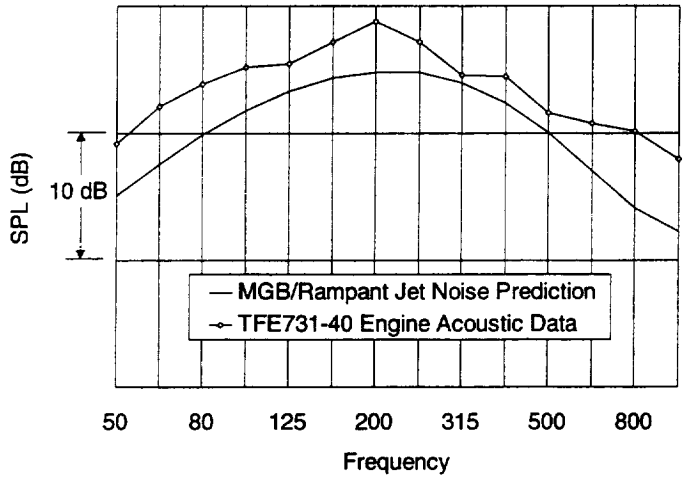

(c) 160 degrees from inlet

Figure 10. Takeoff Power MGB Sound Pressure Level Calculations Have Been Made for the TFE731-40 Baseline Nozzle.

Flowfield analysis. A RAMPANT analysis of the nozzle flowfield was performed at two static performance cycle points, sideline take-off and cutback power. These points are matched to test points for the TFE731-60 engine where acoustic data exists from the Acoustic Test Facility. Due to the axial periodic symmetry of the mixer lobes and ducts of this mixer the model was evaluated as a 1/2 lobe model which incorporates 1/28 of the total flowfield. The mixer flowfield is modeled in RAMPANT with a three dimensional flowfield wedge which contains a half-lobe element of the periodic mixer design with symmetry boundary conditions. To keep reasonably sized computational grids, the problem was divided into a nearfield nozzle calculation and a farfield plume calculation. The interface was set inside the nozzle to ensure that no flow information was lost in the transition between the two grids. this two-step gridding process provides a dense grid for resolving details inside the nozzle and detailed plume definition.

A 12.857° wedge was created using the mixer lobe IGES file information. For the RAMPANT interior analysis, a circular farfield was created around the nozzle exit that was five nozzle exit diameters wide. The mesh and corresponding boundaries are shown in Figure 11. For the boundary conditions, the core and bypass inlets were set as total pressure inlet boundaries with the total temperature and total pressure inputs from the appropriate engine thermodynamic cycle. Since the cycle point is a static point, the farfield was set as a pressure outlet boundary. The walls were set as nonslip and adiabatic and the sides are modeled as symmetry. The mesh was adapted to y^+ to get proper boundary layer definition, gradients of static pressure to get improved shock and flowfield definition, and gradients of total temperature to get improved mixing plane definition. The final mesh size used for the internal flow evaluation was 155 000 fluid cells. A similar process was used to get the interior solution for the cutback power case. The cutback power case was run to 200 000 fluid cells.

The mesh for the plume solution is also shown in Figure 11. The length of the mesh is 50 nozzle exit diameters and the height of the mesh is 11 nozzle exit radii. The boundary conditions used for the analysis were a pressure outlet for the farfield, pressure inlet for the nozzle entrance, symmetry for the sides, and no-slip adiabatic walls. The high power model used ~100 000 fluid cells and was adapted to gradients of static pressure, Reynolds stress and fluid shear (dU/dy).

The connection point between the interior and the plume models is engine station 268.991, which is located several inches upstream of the nozzle throat. This location was chosen to allow proper supersonic flow effects to be properly modeled in the plume. The flow parameter profile (total and static pressure, total temperature, flow component directional cosines, TKE and dissipation) was created using a Fluent Inc. supplied scheme function that creates a file which stores these flow parameters for a defined surface.

Profiles of total temperature contours are shown in Figure 12. This picture shows the effects of flow thermal mixing throughout the nozzle. The TKE levels produced by the mixer within the nozzle are less than 4000 ft^2/sec^2, which is significantly less than the peak levels found in the plume (30 000 ft^2/sec^2). This appears to indicate that jet noise acoustic levels may not be sensitive to mixer design other than how the mixer design affects mixing efficiency and thus the shearing velocities in the plume.

Nozzle performance results of the CFD analysis are shown in Table 1. This data shows that the RAMPANT predictions for thrust and flow are high compared to the cycle predicted values. This is mostly attributed to applying fan exit conditions for the bypass duct but not fully modeling the full bypass duct length (see Figure 11). The bypass duct was shortened to allow greater cell definition in the nozzle mixing region while maintaining the 200 000 fluid cell limit on the mesh. Also of interest is the thermal mixing efficiency, which RAMPANT calculates at 45-47 percent for the 14-lobed mixer. This is significantly lower than thrust-derived thermal mixing efficiency calculated from rig data on the -60 mixer design, but consistent with past RAMPANT CFD runs.

The RAMPANT results are used to calculate the thermal or mass mixing efficiency based on the following equations

$$\eta_{mix} = 1 - \frac{\Delta T_{mean}}{\Delta T_{max}}$$

where:

$$\Delta T_{mean} = \frac{\sum_{i=1}^{n} \dot{m}_i \left| T_{i\ throat} - T_{mave} \right|}{\dot{m}_c + \dot{m}_b}; \qquad T_{mave} = \frac{T_c \dot{m}_c + T_b \dot{m}_b}{\dot{m}_c + \dot{m}_b}$$

$$\Delta T_{max} = \frac{\dot{m}_c \left| T_c - T_{mave} \right| + \dot{m}_b \left| T_b - T_{mave} \right|}{\dot{m}_c + \dot{m}_b}$$

Figure 13 shows the TKE levels for the sideline and cutback power cases. These plots show for the high power case (take-off condition) that the peak levels of TKE are 25% lower than the levels found from the high power TFE731-40 compound nozzle case. The cut power case has 35% lower TKE levels than the high power case but maintains the same TKE plume shape as the high power case. The results of these calculations were then used in the MGB program to compute the far field radiated noise.

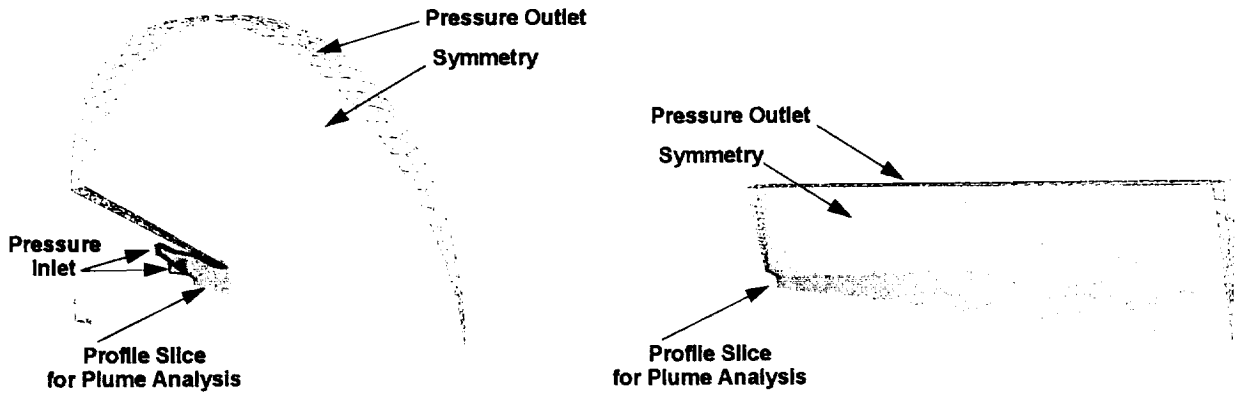

(a) Nozzle flow calculation (b) Plume flow calculation

Figure 11. RAMPANT Computational Grids for -60 Mixer Calculations.

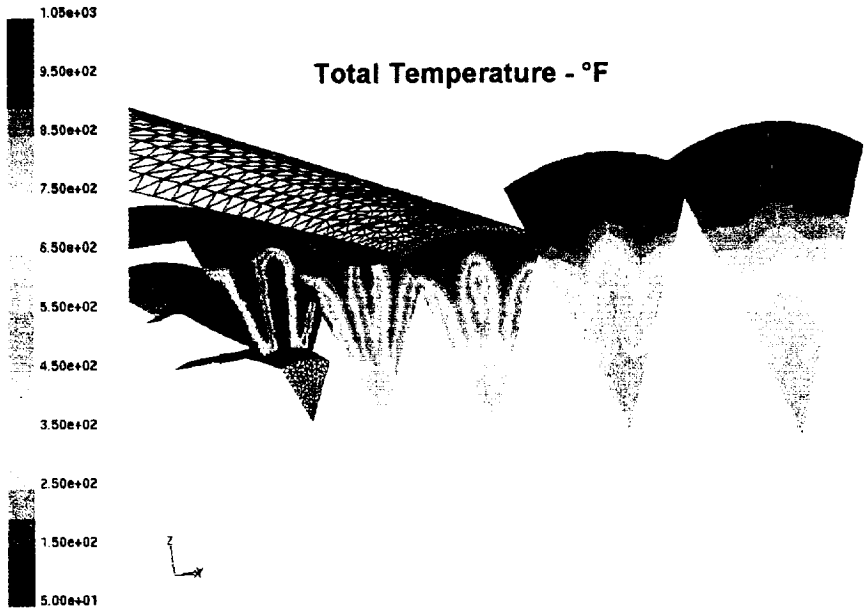

Figure 12. Total Temperature Contours Computed in RAMPANT Show Mixing Effectiveness for the -60 Mixer.

Table 1. TFE731-60 High and Cut Power Mixer Nozzle Performance.

Input Parameters	TFE731-60 Hi-Power	TFE731-60 Cut-Power
Ambient Temperature (°F)	57.6	56.6
Ambient Pressure (psia)	14.115	14.0119
Free Stream Mach Number	0	0
Core Total Temperature (°F)	1031.9	944.2
Bypass Total Temperature (°F)	143.4	114.3
Core Total Pressure (psia)	21.36	17.83
Bypass Total Pressure (psia)	22.301	19.162
Cycle Parameters		
Core Massflow (lbm/sec)	33.182	22.834
Bypass Massflow (lbm/sec)	136.87	114.97
Total Massflow (lbm/sec)	170.052	137.804
Thrust (lbf)	5352	3339
RAMPANT Calculated Parameters		
Core Massflow (lbm/sec)	31.7234	21.616
Bypass Massflow (lbm/sec)	141.569	119.919
Total Massflow (lbm/sec)	173.2924	141.535
Pressure Thrust (lbf)	-568.5	-133.24
Momentum Thrust (lbf)	6023.37	3582.25
Total Thrust (lbf)	5454.87	3449.01
Thermal Mixing Efficiency	0.4761	0.45774
Mass Ave Total Pressure Loss	0.02883	0.0202

Since the MGB code assumes an axisymmetric flowfield, the azimuthal flowfield variation cannot be included in the MGB input. A procedure for interpolating the 3-D unstructured grid has been developed for the axisymmetric structured grid of MGB. Three jet noise predictions were made for the 14-lobe TFE731-60 mixer nozzle at the high power condition. Data was extracted from the RAMPANT CFD solution along three different slices of the jet plume. The 3-D RAMPANT geometry is a 12.857-degree wedge containing half of a mixer lobe. The slices on which the data was extracted are at a constant azimuthal location and run axially down the length of the plume. They are referred to as the "top", "median", and "bottom" lobe slices. Only data downstream of the nozzle exit is used in the noise calculation. These slices cut through numerous cells along the mid-lobe plane, and thus generate a collection of coordinates and corresponding flowfield values. This data is interpolated onto a structured grid

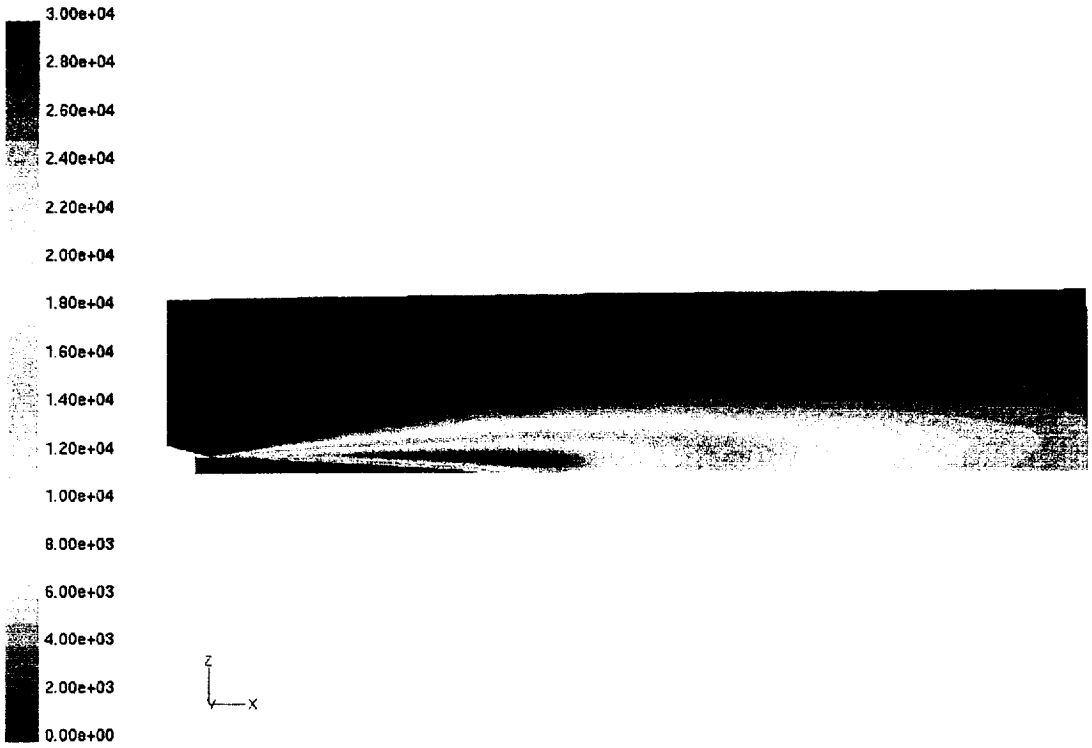

(a) Sideline power case

(b) Cutback power case

Figure 13. Contours of Turbulent Kinetic Energy Show the Effect of Engine Power Setting on the Jet Plume Turbulence Structure.

measuring 174 grid points in the axial direction by 118 grid points in the radial direction. The structured grid was more heavily refined along the nozzle exit line and at the jet exit plane to better resolve shear layer and near-field variations. Figure 14 shows that the computed noise is quite insensitive to the position of the 2-D slice.

RAMPANT CFD results were generated for the TFE731-60 nozzle at both full and cutback power points Figure 15 shows comparisons between the predicted power levels and engine acoustic data for the full and cutback power cases respectively. Note that the magnitude of the peak power level and the frequency at which it occurs are both overpredicted. The reason for the discrepancy is not understood and may point to a limitation of the RAMPANT CFD results, the axisymmetric MGB code, the 3-D to 2-D interpolation process, or a combination thereof. Figure 15 shows a comparison between the predicted and measured sound pressure levels for an angle of 140 degrees from the engine inlet for the high power case. It was at this angle that the predicted SPL for the TFE731-40 was in best agreement with the acoustic data. Note that although the shape is satisfactory, the peak level is overpredicted by about 6 dB.

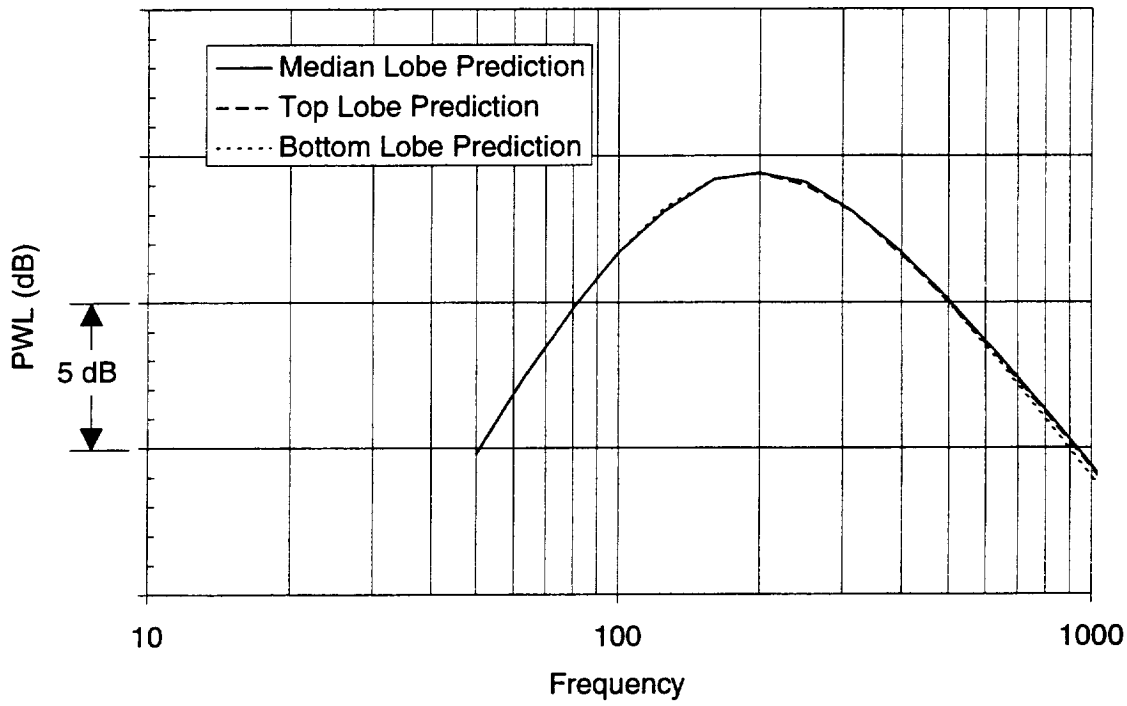

Figure 14. The Circumferential Variation in the MGB Noise Calculation Is Minimal.

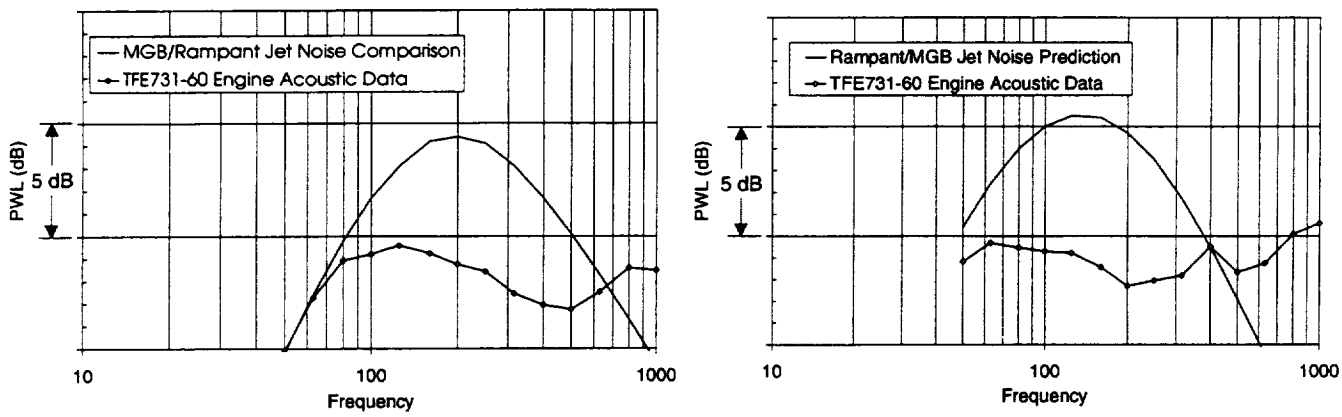

(a) Takeoff Power

(b) Cutback Power

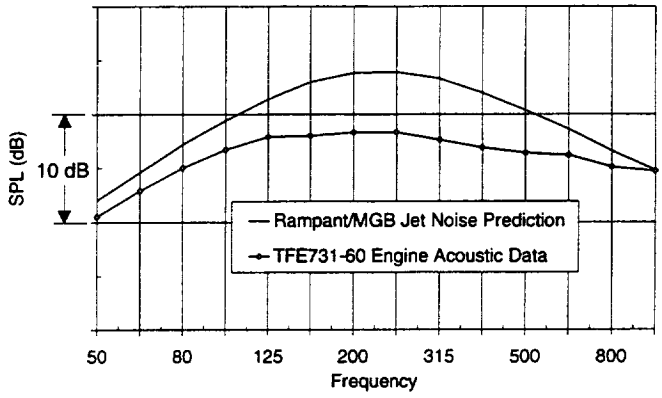

(c) Full power SPL at 140 degrees from inlet

Figure 15. The Predicted Acoustic Power for the TFE731-60 Mixer Nozzle Shows Less Satisfactory Agreement with the Measured Engine Data than the TFE731-40.

3.4 Design Tool Validation

The V2 nozzle configuration from the E^3 study was been selected for validation of the AE CFD and computational aeroacoustic analysis. The geometric, aerodynamic, and noise data from the model tests conducted by GE Aircraft Engines (Reference 3) have been received from NASA Lewis in electronic files. Figure 16 shows a diagram of the mixer configuration.

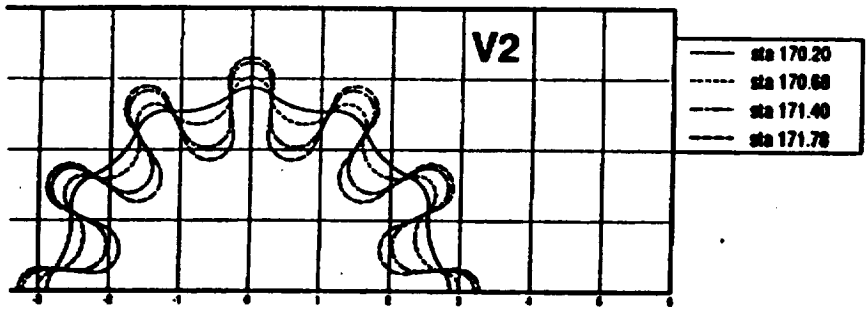

Figure 16. Diagram Shows the Lobe Configuration of the V2 Mixer from the E^3 Study.

CFD Model. The E^3 V2 mixer was evaluated at two static operating conditions, test points 5 and 7. For the model, the core and bypass inlets were modeled as pressure inlet boundaries, the farfield modeled as a pressure outlet and the turbulence model used was RAMPANT's base k-ε model. For the analysis, a one half-lobe model was evaluated. The RAMPANT mesh used for the analysis is shown in Figure 17. The final adapted mesh contained over 200 000 fluid cells and was adapted to gradients of total temperature, static pressure, and wall y^+. Boundary condition values used for the interior CFD model are shown in Table 2.

Table 3 outlines the thrust, flow and mixing performance for the E^3 mixer configurations. From this table, the thermal mixing efficiency for this nozzle is approximately 50 percent, which is about 15 percent lower than the efficiencies calculated for the advanced mixer designs presented in the next chapter. Figure 18 shows temperature contours at various cuts through the nozzle rig mixing section. This plot illustrates how well thermal mixing occurs downstream of the mixing plane. These runs also allowed comparison of the CFD results to experimental data as discussed below.

The plume was modeled using a temperature and pressure profile generated from the interior solution. The axial location for the generated profile was at rig station 174.5. The mesh used to generate the plume solution contained over 90 000 fluid cells and was adapted to gradients of static pressure, total temperature, dU/dy, and Reynolds stress. For the solution, RAMPANT's standard k-ε model was used. The farfield mesh was modeled out to 25 nozzle exit diameters downstream of the nozzle exit and the farfield height was greater than 10 nozzle exit radii. Figure 19 shows the TKE plume for the mixer lobe peak symmetry surface. Peak TKE levels (29 000 ft^2/s^2) are less than values seen for AE's advanced mixer configurations (31 000-34 000 ft^2/s^2). This difference is expected due to the higher bypass ratio of the E^3 testing.

Table 2. Boundary Conditions Used for E^3 Mixer Nozzle Analyses.

	Test Case 5	Test Case 7
Ambient Temperature, F	40	33.9
Ambient Pressure, psia	14.32	14.572
Core Total Pressure, psia	23.485	25.6904
Core Total Temperature, F	984	1029.8
Core Inlet TKE, ft^2/s^2	95	95
Core Inlet Dissipation, ft^2/s^3	3 060 000	3 060 000
Bypass Total Pressure, psia	22.912	24.8861
Bypass Total Temperature, F	90	72.2
Bypass Inlet TKE, ft^2/s^2	40	40
Bypass Inlet Dissipation, ft^2/s^3	1 670 000	1 670 000

Table 3. RAMPANT Predicted E^3 Performance Values for V2 Mixer Test Cases.

	Test Case 5	Test Case 7
Core Airflow, lbm/sec	2.425	2.674
Bypass Airflow, lbm/sec	16.965	19.084
Total Airflow, lbm/sec	19.391	21.758
Pressure Thrust, lbf	75.282	95.293
Momentum Thrust, lbf	511.327	598.955
Total Thrust, lbf	586.609	694.248
Thermal Mixing Efficiency	0.509	0.514
Mass Ave Pressure Loss	0.025	0.027

Exit Rake Total Temperature and Pressure Comparison. Exit rake total temperature and total pressure data for Test Cases 5 and 7 were measured during the V2 nozzle rig testing. Figure 20 shows the measurement grid for the exit rake measurements. Figures 21 and 22 show the measured normalized total temperature and pressure contours for test case 5 and 7, respectively, at the nozzle exit plane. Figures 23 and 24 show the equivalent RAMPANT CFD generated normalized total temperature and pressure contours for the two cases.

Figure 17. E^3 Rig Surface Mesh Used in the RAMPANT CFD Analysis Was Modeled Using the Same Procedure as the TFE731-60.

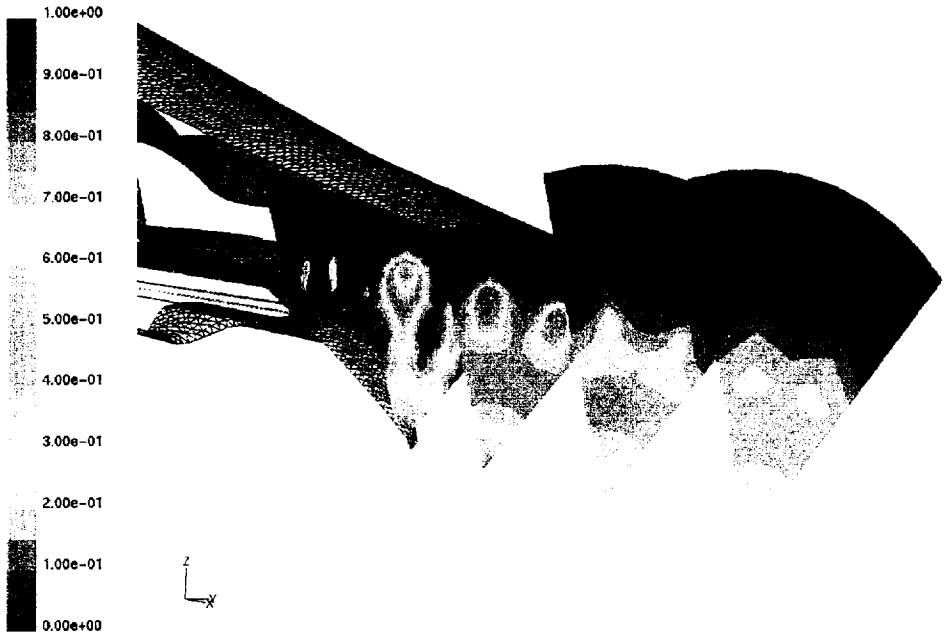

Figure 18. Normalized Temperature Contours at Various Axial Coordinates Show the Thermal Mixing for the V2 Mixer at Test Case 7 Conditions.

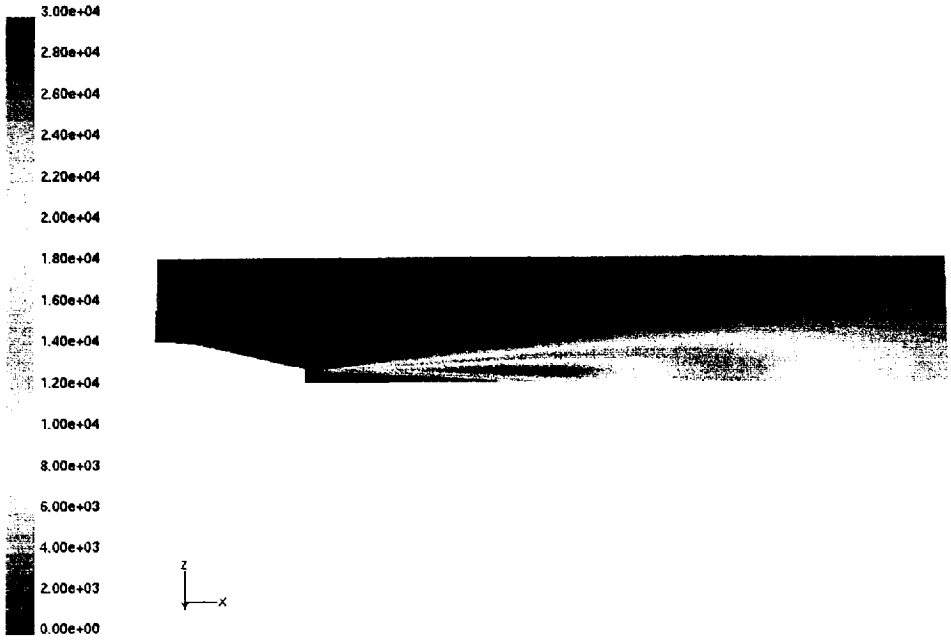

Figure 19. TKE Plume Contours Have Been Computed for Test Case 7 of the V2 Mixer Evaluation.

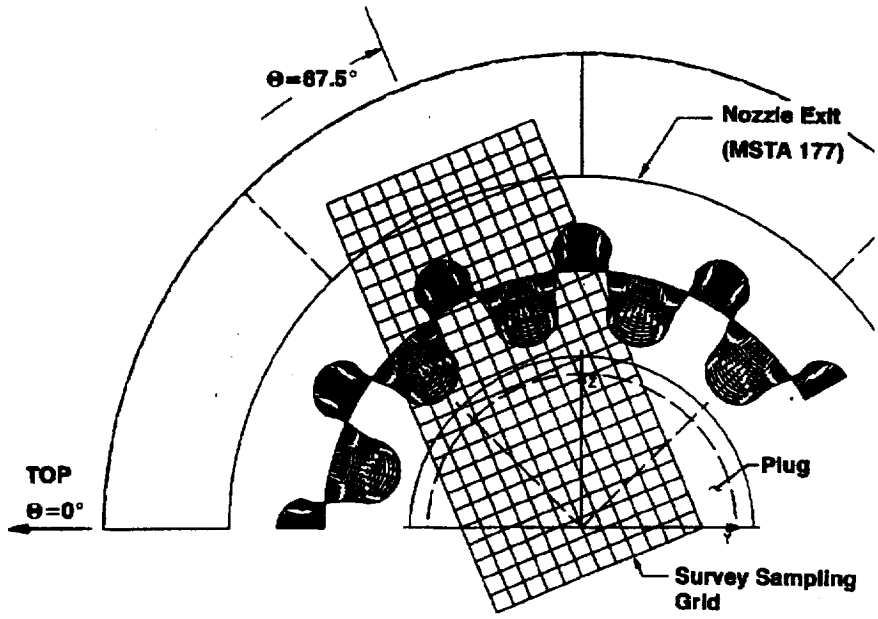

Figure 20. The Survey Grid for the Exit Total Pressure and Temperature Measurements on the E^3 Mixer

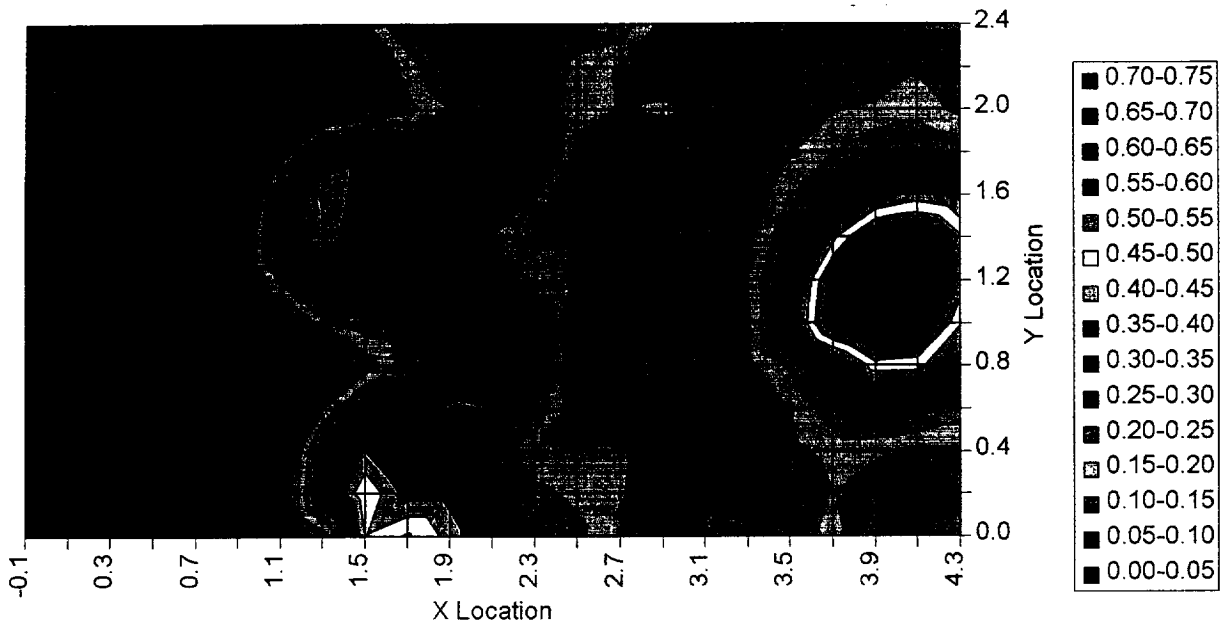

(a) Normalized total temperature

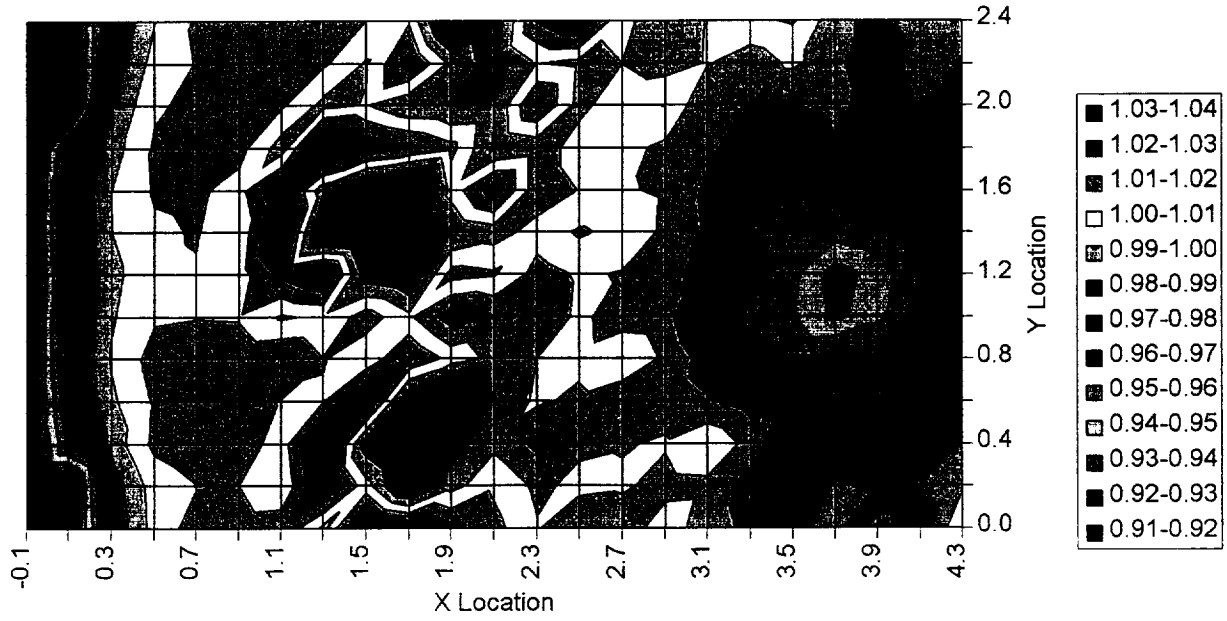

(b) Normalized total pressure

Figure 21. Measured Total Pressure and Temperature Data at the Nozzle Exit for Test Point 5 is Available for Prediction Comparisons.

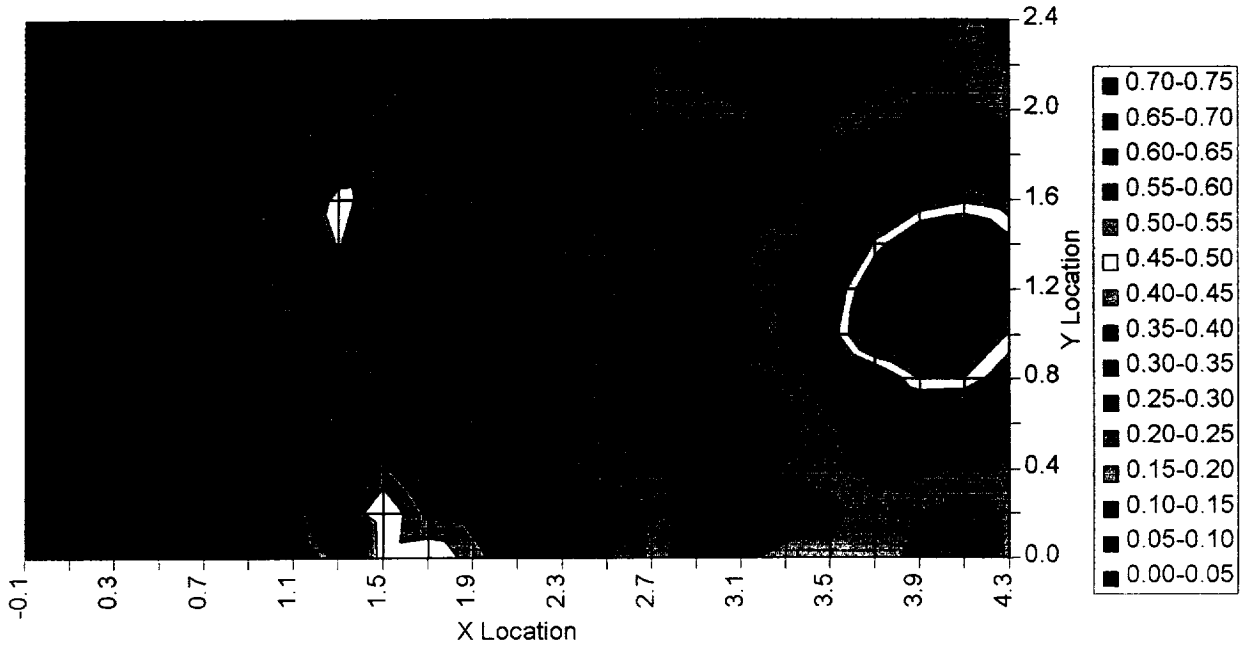

(a) Normalized total temperature

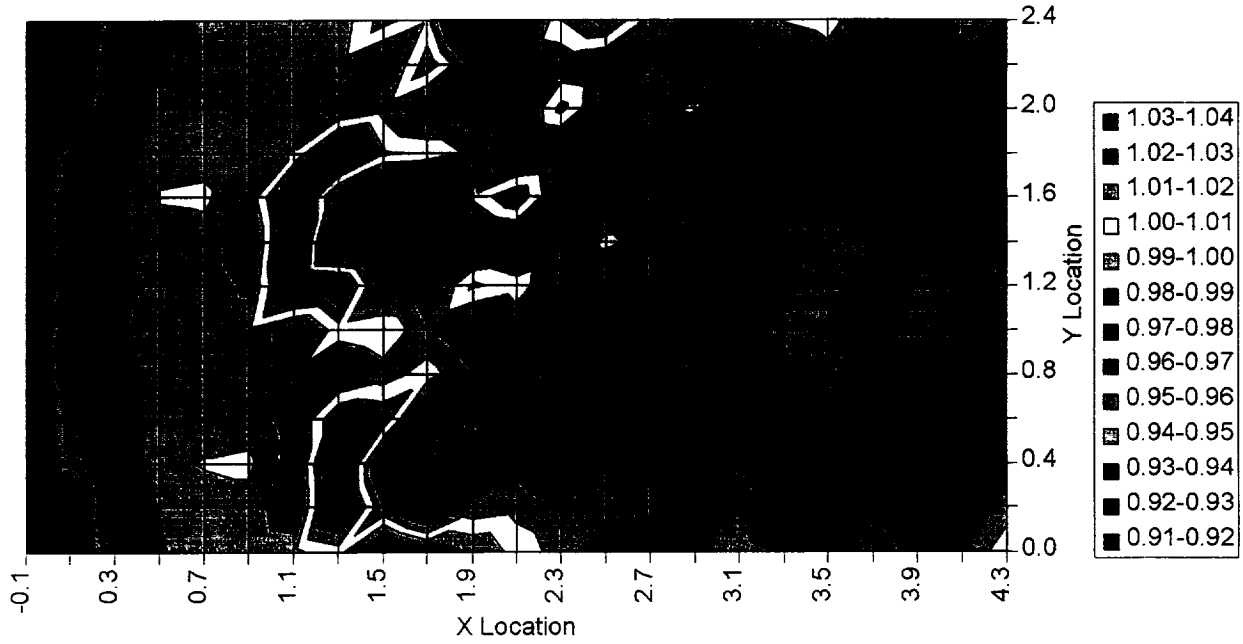

(b) Normalized total pressure

Figure 22. Measured Total Pressure and Temperature Data at the Nozzle Exit for Test Point 7 is Available for Prediction Comparisons.

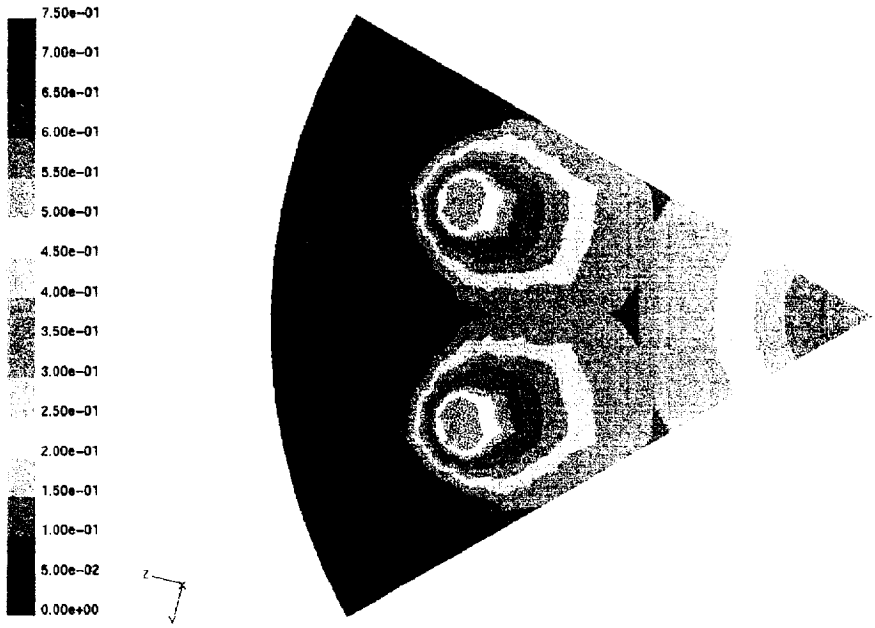

(a) Normalized total temperature

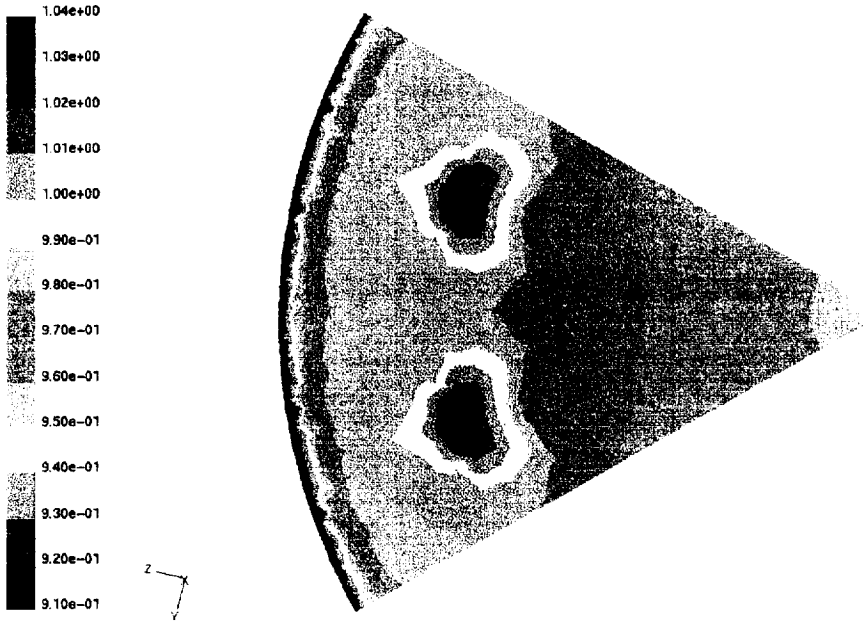

(b) Normalized total pressure

Figure 23. The Comparison of the RAMPANT Predicted Total Pressure and Temperature with the Measured Data at the Nozzle Exit for Test Point 5 Shows the Accuracy of the Prediction.

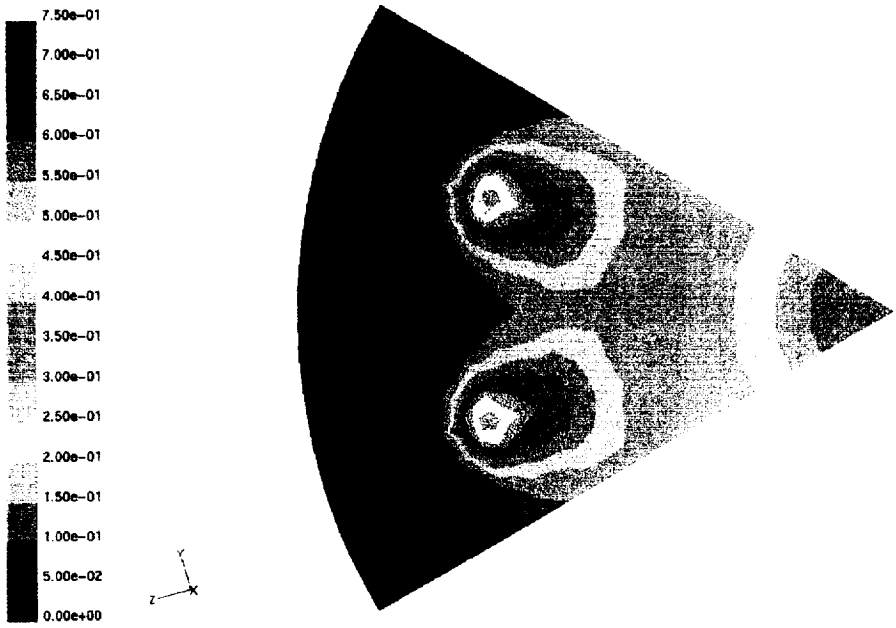

(a) Normalized total temperature

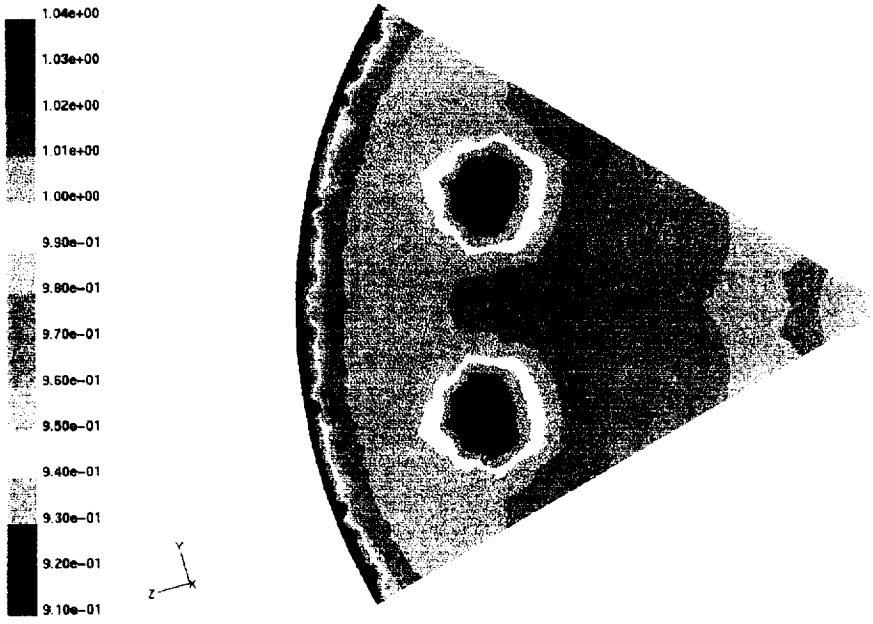

(b) Normalized total pressure

Figure 24. The Comparison of the RAMPANT Predicted Total Pressure and Temperature with the Measured Data at the Nozzle Exit for Test Point 7 Shows the Accuracy of the Prediction.

For this evaluation, the normalized total temperature is defined as:

$$T_{t\,norm} = (T_t - T_{t\,bypass}) / (T_{t\,core} - T_{t\,bypass})$$

The normalized total temperature plots show that RAMPANT modeled the peak lobe temperature within 5 percent of the measured values (< 0.5 for test, < 0.55 for RAMPANT) and that the lobe hot spot is somewhat circular. RAMPANT did not properly predict the extremely hot centerline temperatures seen in both sets of test data (<0.75 for test, <0.40 for RAMPANT). The reason for the extremely hot centerline temperatures is not known.

For this evaluation normalized pressure is defined as

$$P_{t\,norm} = P_t / P_{t\,bypass}$$

The normalized total pressure plots show RAMPANT did not effectively model the lobe total pressure distribution since RAMPANT predicted a round peak pressure region while the test data showed a crescent shaped peak pressure region. This result indicates that either the half-lobe symmetry assumption is not valid where significant flow crosses the 1/2 lobe symmetry boundaries in the test model or insufficient mesh detail was obtained in the analysis.

For the LDV data comparison to the RAMPANT results, plots of mean axial and vertical velocities were made for the rig test and RAMPANT CFD analysis. LDV data was taken at seven locations in the nozzle/plume for Test Case 5, as shown in Figure 25. Figures 26 to 33 show the axial and vertical mean velocity contours for the test rig measurement and RAMPANT analysis at the various axial test locations. Comparison between LDV measured mean velocities and RAMPANT predicted values are generally good for axial velocities. However, measured axial velocities at Station 176 (Figure 27) show the same crescent shape characteristics as the nozzle exit total pressure contours indicating that the axial velocity is driven by the total pressure. RAMPANT-confuted vertical velocities do not compare well with the LDV data after Station 173 where mean vertical velocities are in the same order of magnitude as the turbulent velocities. The comparable figures were plotted to the same range of values in order to assist in the visual comparison between rig and CFD values.

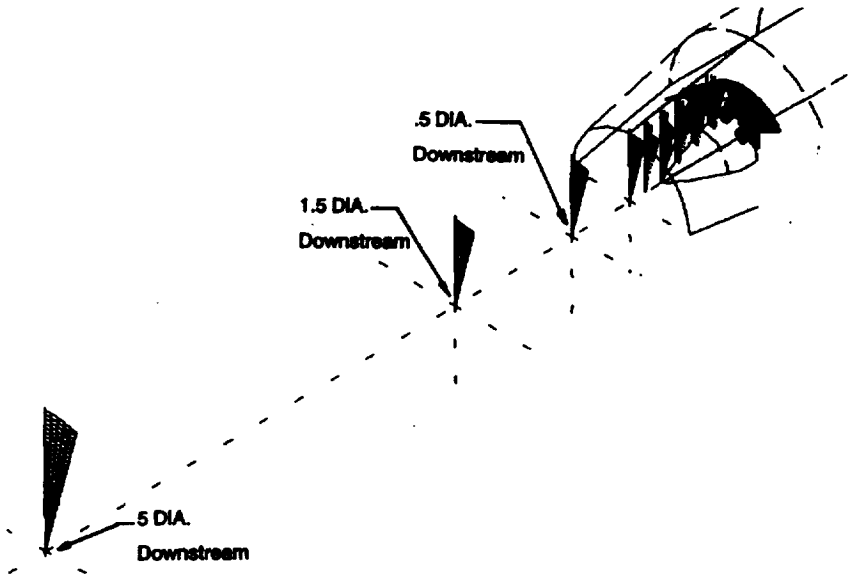

Figure 25. Diagram Shows the Position of the LDV Measurements of the V2 Mixer for the E^3 Study.

Acoustic evaluations were performed for two static test cases, Test Points 5 and 7, for the V2 scalloped mixer (also referenced as acoustic test points 181 and 183). The mixer, which has 12 lobes, was evaluated within RAMPANT on a 3-D wedge of 15 degrees using symmetry boundary conditions for the wedge sides. The plume solution contained over 90 000 fluid cells. Jet plume flowfield data from the wedge was interpolated onto a structured grid for use in the MGB code. The structured grid measured 174 points axially by 119 points radially. Using a FORTRAN code, the data was sorted, interpolated, nondimensionalized, and organized into input files for use by MGB. The resulting predictions (for a 40 ft. arc) were compared to model scale acoustic data. No sound power levels were computed in the model scale acoustic data obtained by AE, so only sound pressure levels were compared. Figures 34 and 35 compare the sound pressure levels measured at 120 and 140 degrees from the jet inlet. Two MGB predictions were generated, one using the default value of 0.325 for the input parameter BETAMC and one using the value of 0.2, which in the case of the TFE731-40, provided a better match between the data and prediction. Note that the MGB predictions tend to have a characteristic "hill" shape, and the peak SPLs and the frequency at which they occur are overpredicted. Figure 36 shows a comparison of the predicted and measured overall sound pressure levels. It is interesting to note that by reducing the value of BETAMC, the downstream radiated noise is intensified and the upstream radiated noise is reduced. Figures 37 to 39 display corresponding comparisons for Test Point 7.

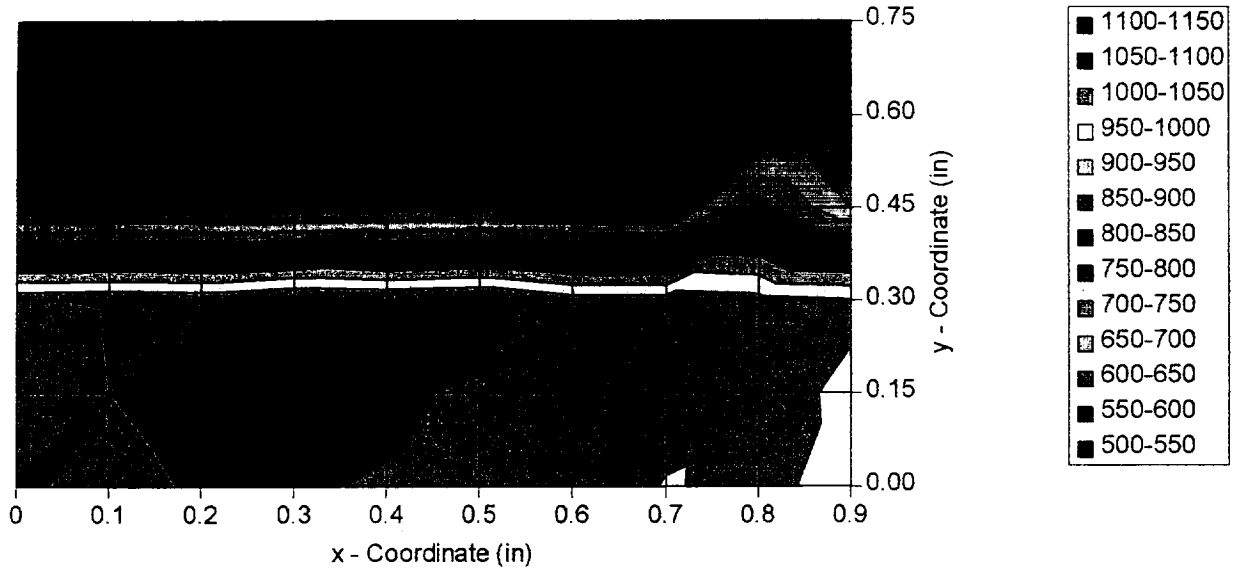

(a) axial velocity

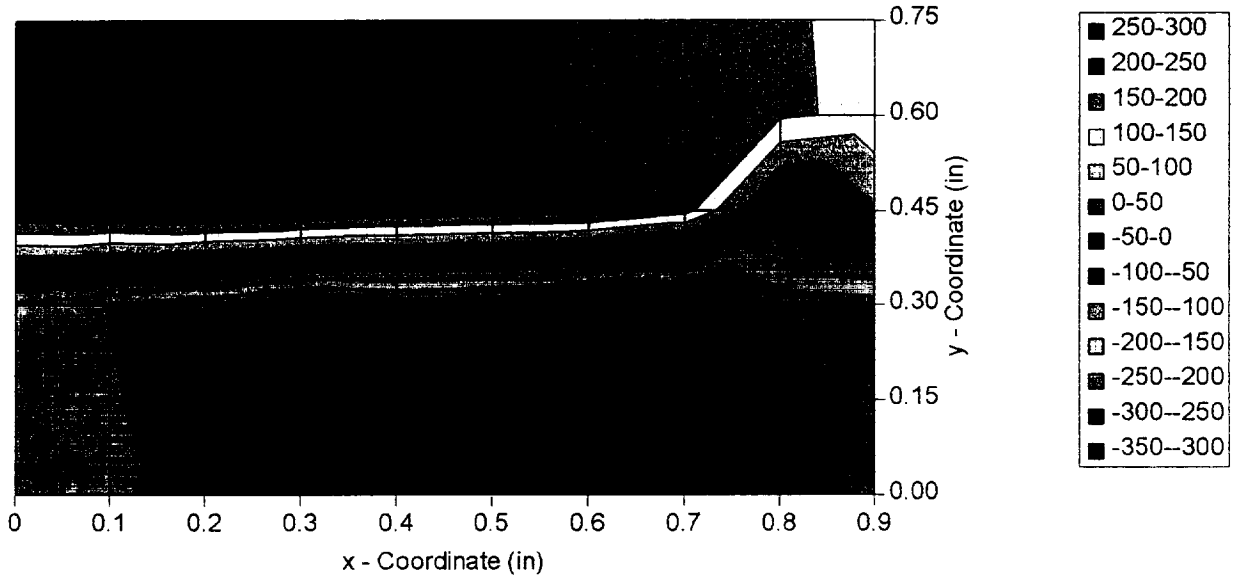

(b) radial velocity

Figure 26. Laser Velocimetry Data Show Flow Characteristics 5 In. Upstream from Nozzle Exit.

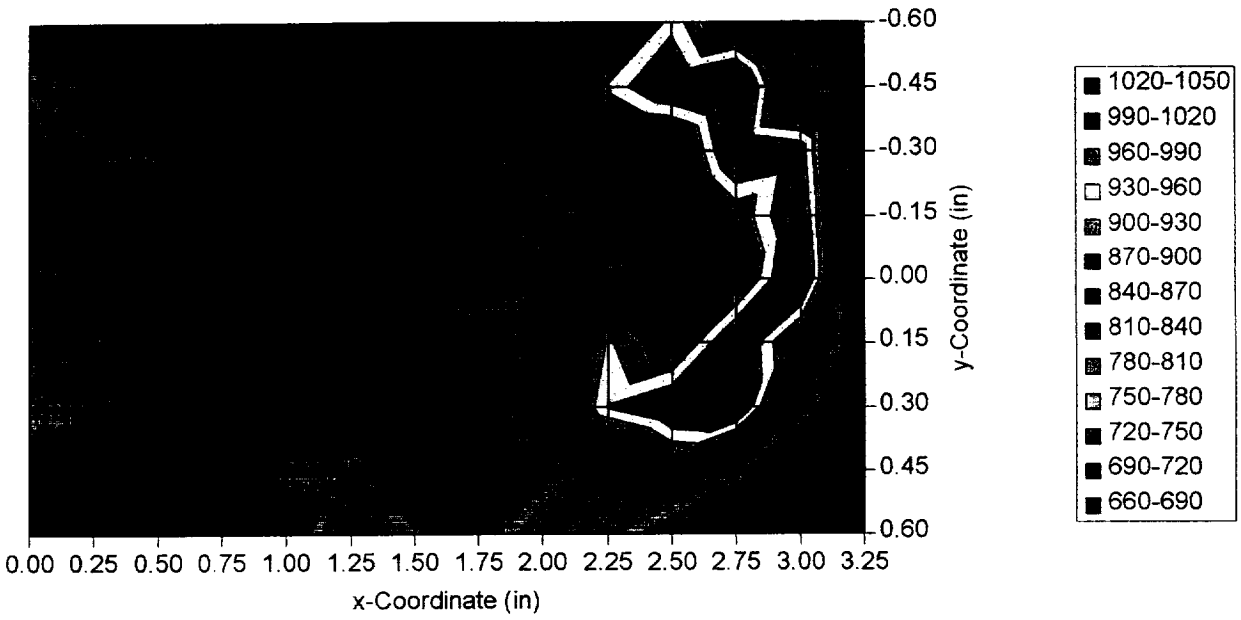

axial velocity

Figure 27. Laser Velocimetry Data Show Flow Characteristics 1 In. Upstream from Nozzle Exit.

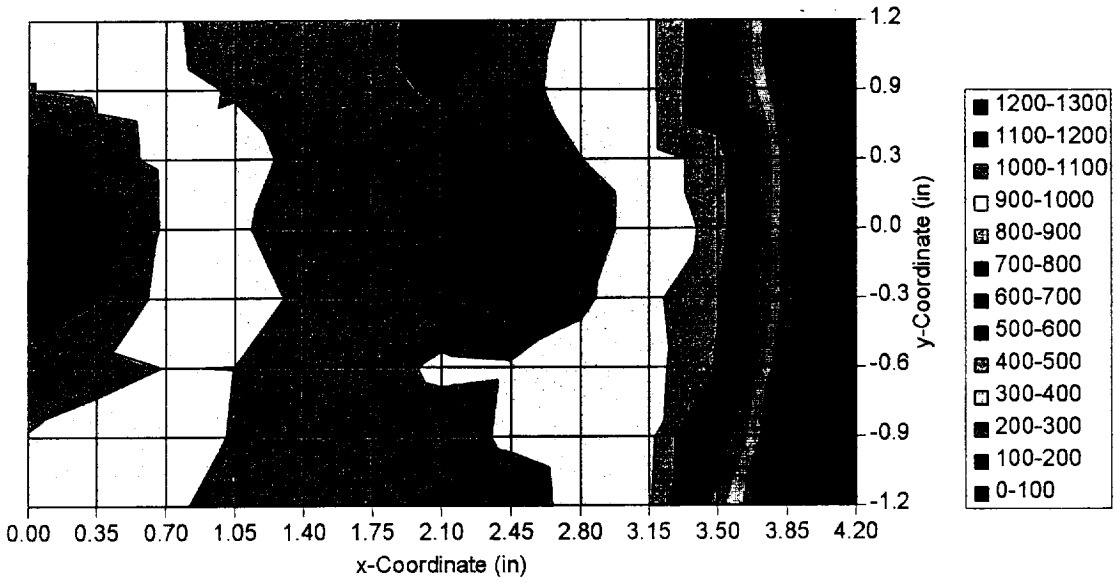

axial velocity

Figure 28. Laser Velocimetry Data Show Flow Characteristics 0.5 Diameters Downstream from Nozzle Exit.

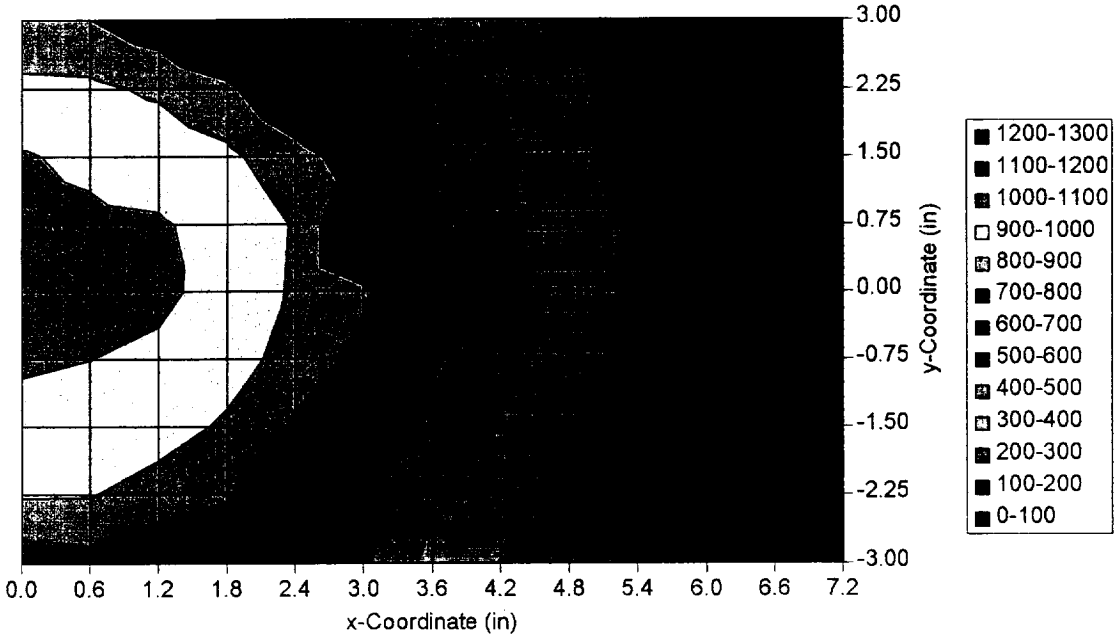

axial velocity

Figure 29. Laser Velocimetry Data Show Flow Characteristics 5 Diameters Downstream from Nozzle Exit.

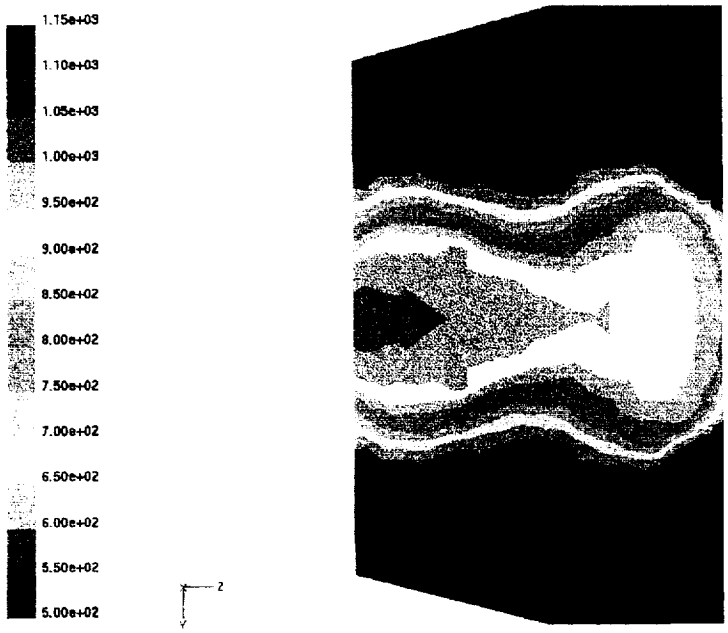

(a) axial velocity

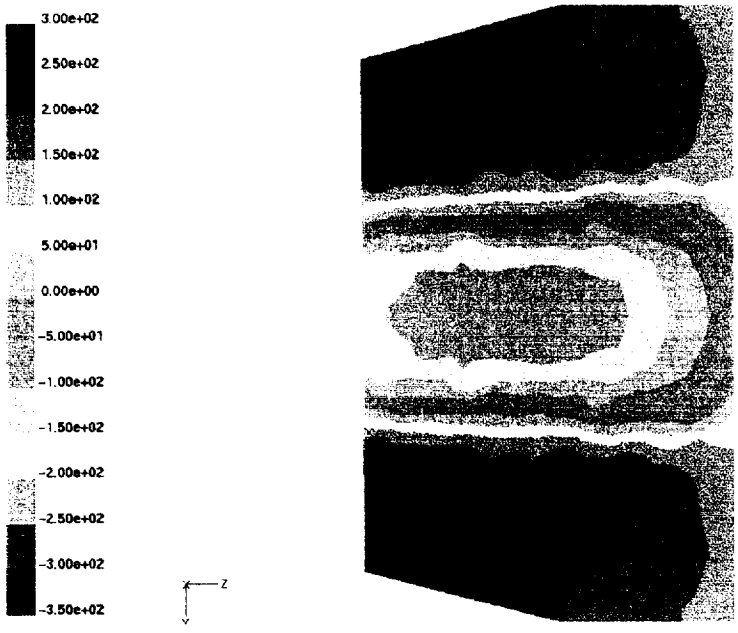

(b) radial velocity

Figure 30. RAMPANT Calculations Can Be Compared to the Laser Velocimetry Data to Show the Flow Characteristics 5 In. Upstream from the Nozzle Exit.

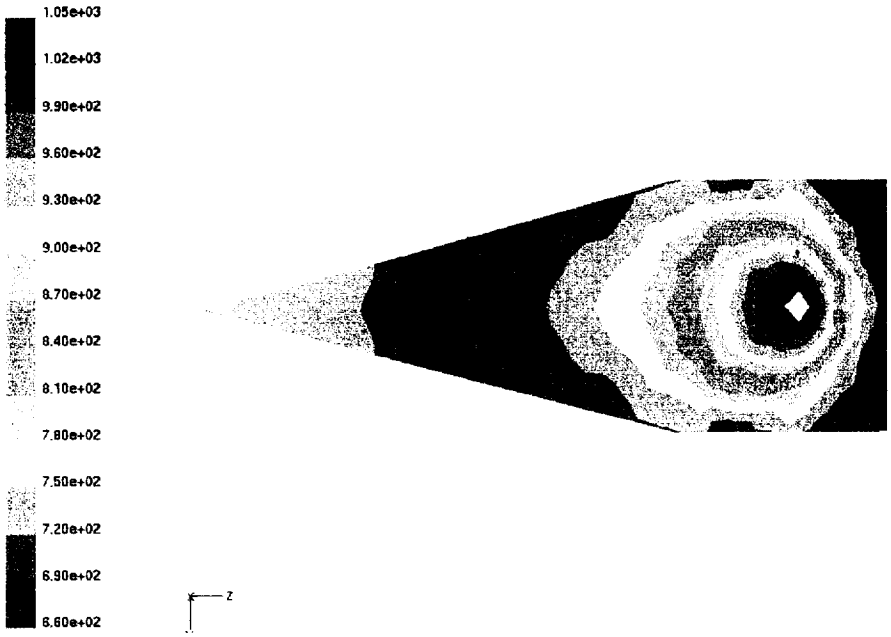

axial velocity

Figure 31. RAMPANT Calculations Can Be Compared to the Laser Velocimetry Data to Show the Flow Characteristics 1 In. Upstream from the Nozzle Exit.

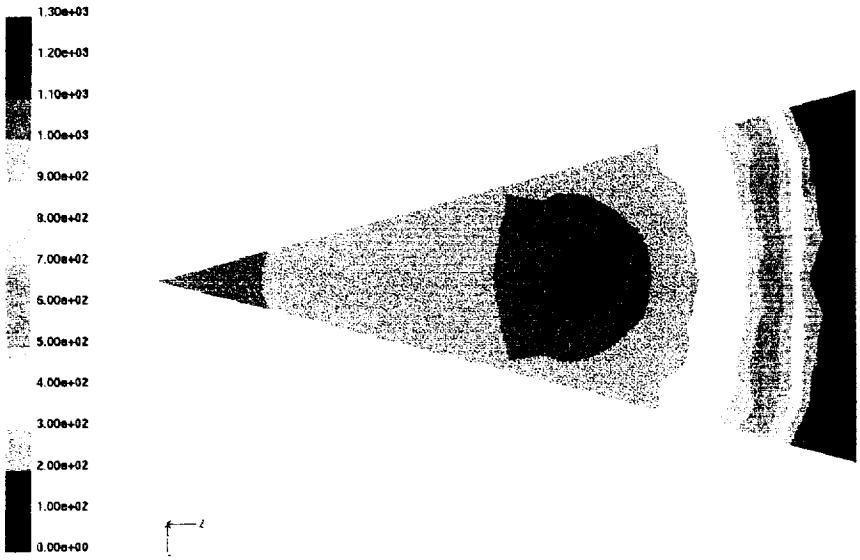

axial velocity

Figure 32. RAMPANT Calculations Can Be Compared to the Laser Velocimetry Data to Show the Flow Characteristics 0.5 Diameters Downstream of the Nozzle Exit.

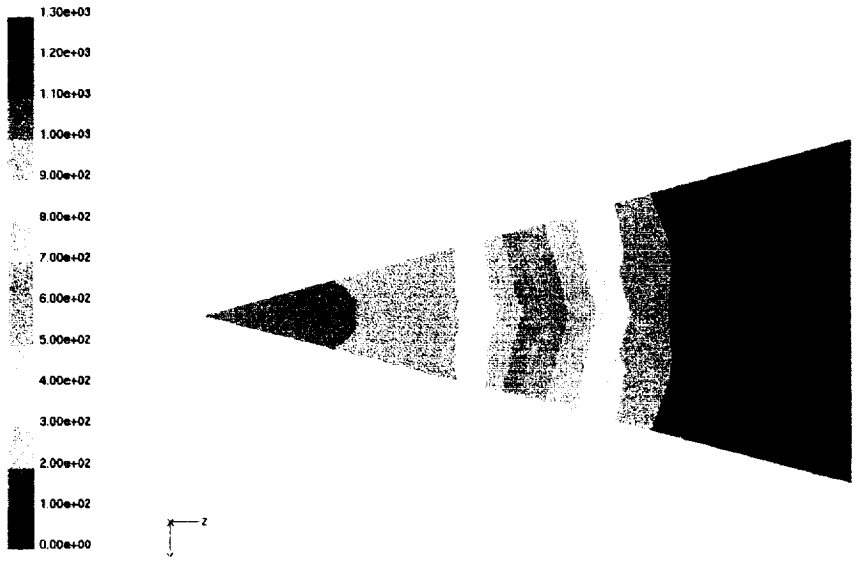

axial velocity

Figure 33. RAMPANT Calculations Can Be Compared to the Laser Velocimetry Data to Show the Flow Characteristics 5 Diameters Downstream of the Nozzle Exit.

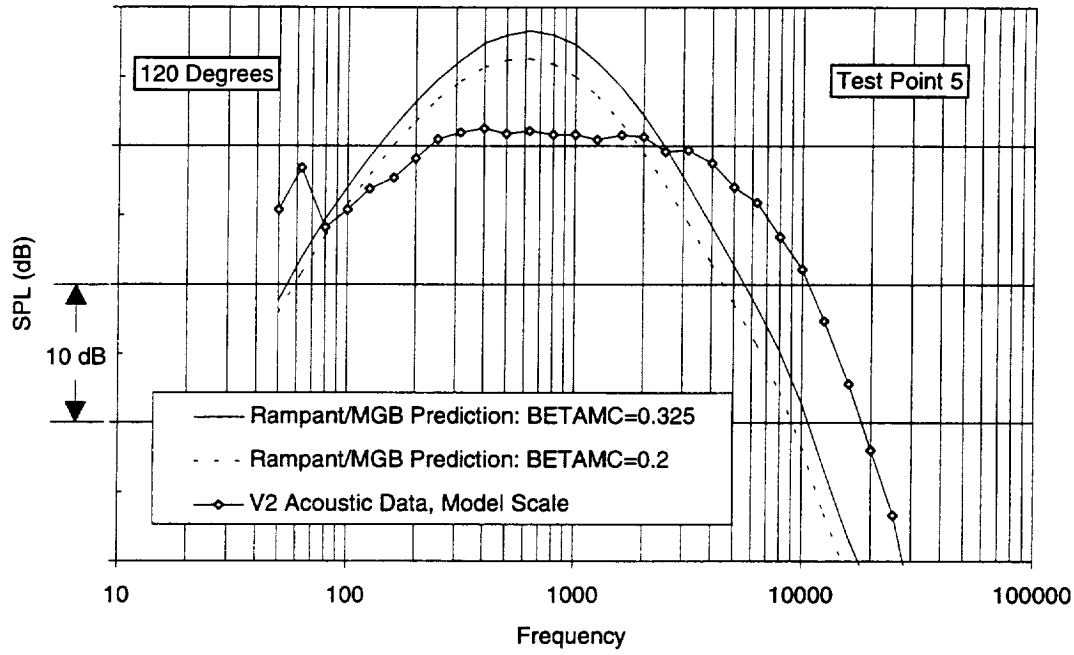

Figure 34. The RAMPANT/MGB Calculations Overpredict the Measured E^3 Mixer Acoustic Data at 120 degrees for Test Point 5.

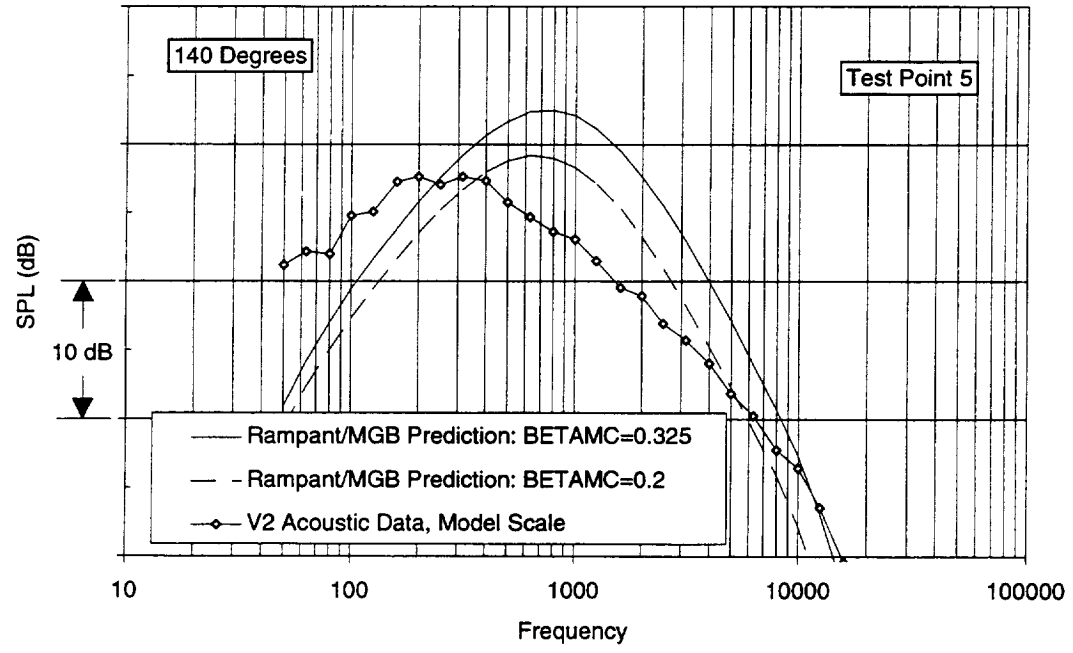

Figure 35. The RAMPANT/MGB Calculations Overpredict the Measured E^3 Mixer Acoustic Data at 140 Degrees for Test Point 5.

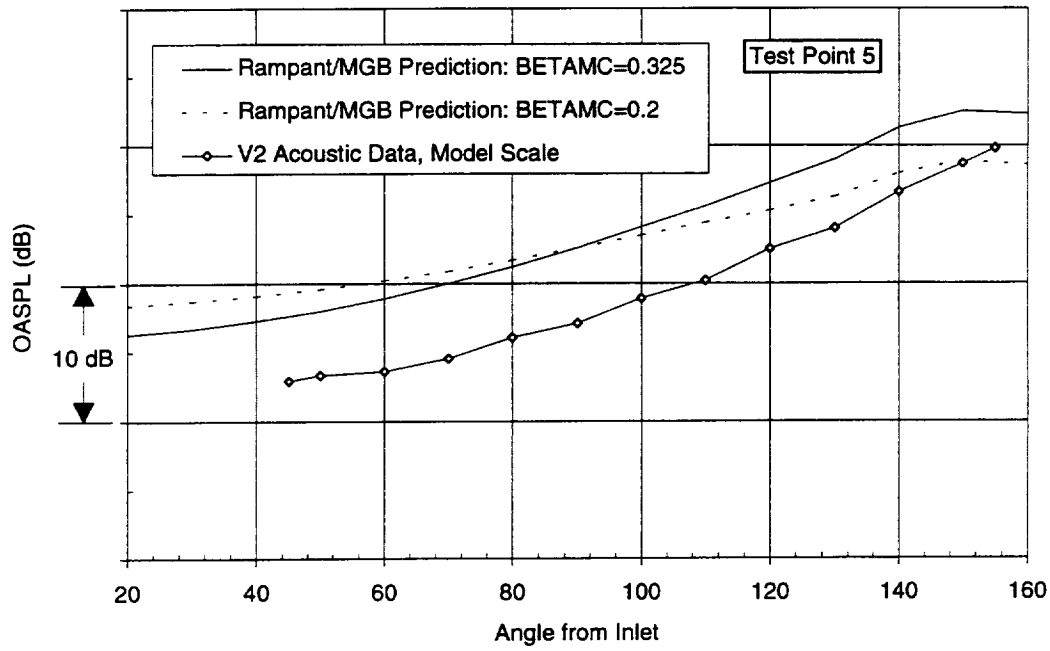

Figure 36. The RAMPANT/MGB Calculations Overpredict the Measured E^3 Mixer Overall Sound Pressure Level for Test Point 5.

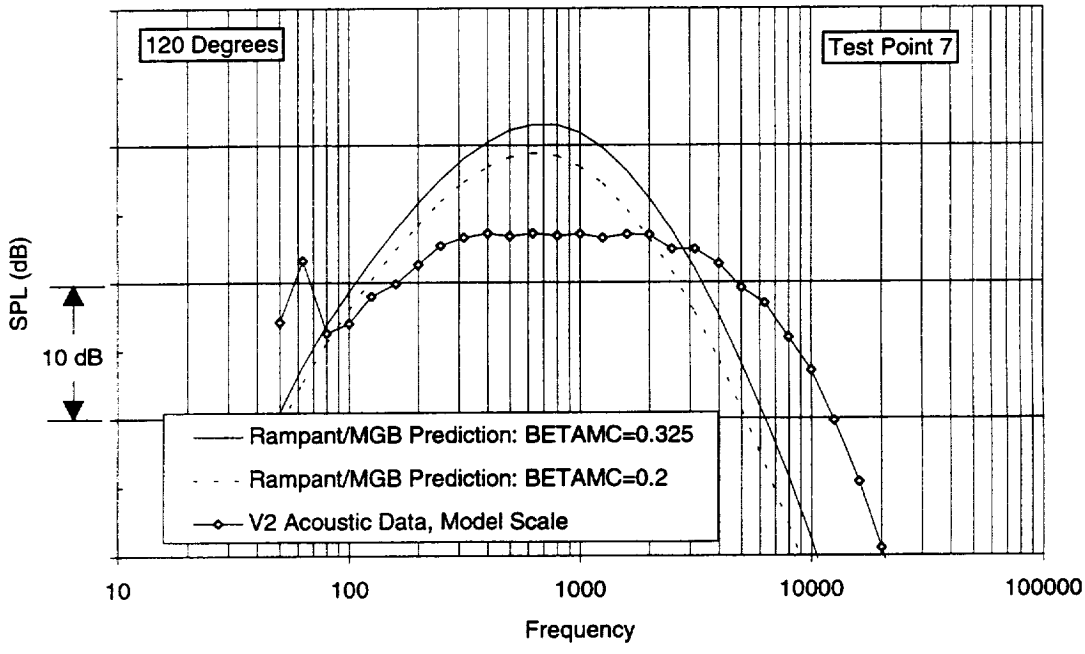

Figure 37. The RAMPANT/MGB Calculations Overpredict the Measured E^3 Mixer Acoustic Data at 120 Degrees for Test Point 7.

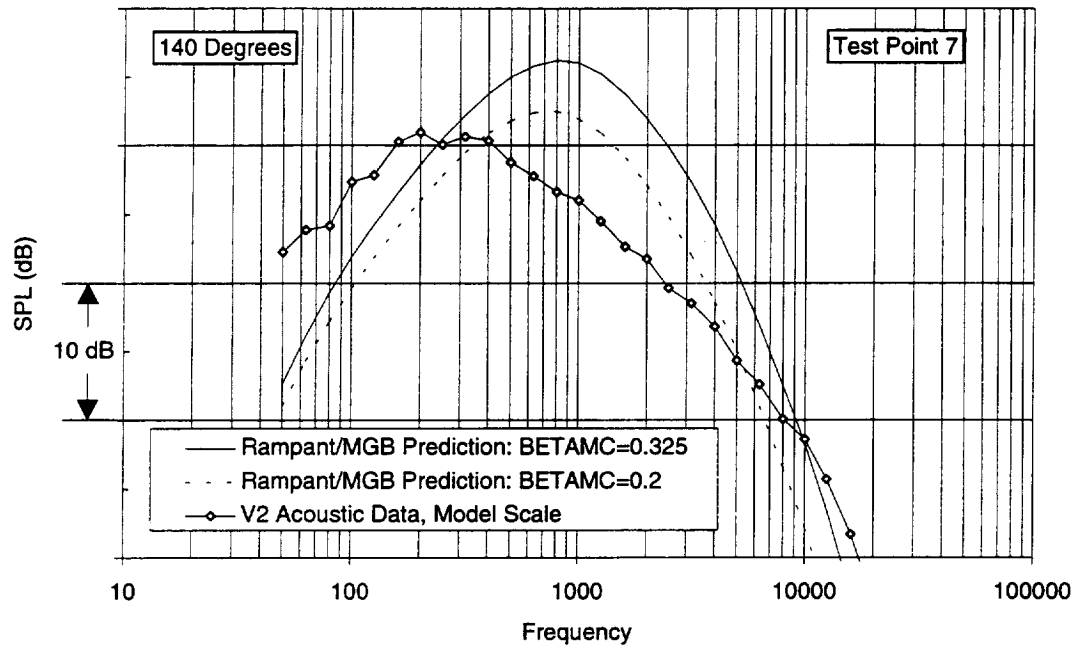

Figure 38. The RAMPANT/MGB Calculations Overpredict the Measured E^3 Mixer Acoustic Data at 140 Degrees for Test Point 7.

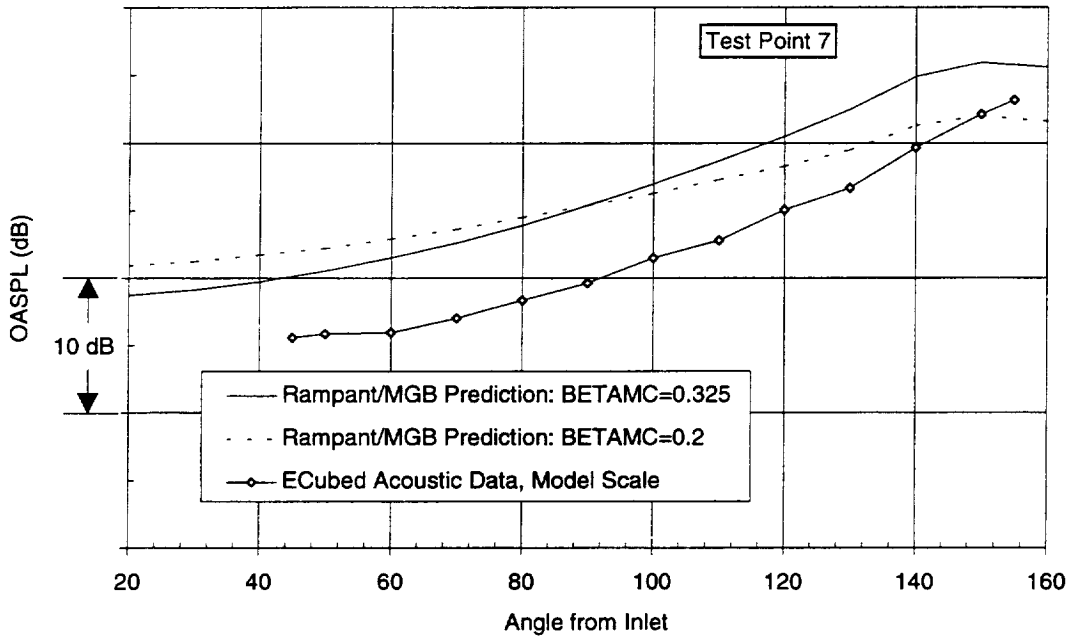

Figure 39. The RAMPANT/MGB Calculations Overpredict the Measured E^3 Mixer Overall Sound Pressure Level for Test Point 7.

3.5 Initial Nozzle Concepts

A design of three innovative mixer concepts has been completed as a part of this study. The designs are based on state-of-the-art design practices, but design parameter values were used that would advance the nozzle performance beyond current design targets. Design parameter values were selected to achieve high mixing efficiency while maintaining the nozzle size within a reasonable envelope. A summary of each mixer concept is provided below.

1) Mixer No. 1 is a high efficiency, 18-lobed conventional design.

2) Mixer No. 2 has the same physical design as mixer No. 1, except that it is manufactured from a porous (probably perforate) material with the equivalent of 10 percent open area.

3) Mixer No. 3 has lobes in the core plug that match up with the mixer lobes.

A high lobe density mixer with 18 mixer lobes was chosen as the first mixer configuration evaluated. This mixer lobe density was selected due to experience obtained from the CFE738 program. Mixer lobe contours and core/bypass flowpaths were designed to achieve an 85 percent mixing efficiency and be shorter in length than existing TFE731 mixer nozzles.

The second mixer selected to be evaluated was the Configuration 1 mixer, but with the mixer modeled as a porous surface. The porous mixer surface, as evaluated in RAMPANT, was modeled using a porous jump boundary condition. A porous jump boundary is modeled as a thin surface, which has a viscous and an inertial pressure drop, where the pressure drop Δp is defined as:

$$\Delta p = -\left(\frac{\mu}{\alpha} V + C_2 \frac{1}{2} \rho V^2\right) \Delta m$$

where μ is laminar fluid viscosity, α is the porosity of the medium, C_2 is the inertial pressure jump coefficient, V is the normal fluid velocity, ρ is the fluid density and Δm is the medium thickness. The porosity and the inertial loss coefficient were calculated using empirical pressure drop correlations for acoustic liners. For this analysis, the open area was assumed to be 10 percent, the hole diameter equal to 0.02 in. and the metal (medium) thickness is 0.045 in.

The third configuration added a core/plug mixer, designed using the same technique as the previous core/bypass mixer. The goal of core/plug mixer design was to improve mixing by bringing more cool bypass air toward the centerline of the nozzle

and thus reducing the hot centerline core flow seen in the TFE731-60 evaluation. Figure 40 shows a 3-D view of each nozzle design and Table 4 shows the design characteristics of each nozzle.

Table 4. Design Characteristics of the Three Innovative Nozzles.

	Configuration 1	Configuration 2	Configuration 3
Objective	Expand current technology	Premix in mixer - core acoustic attenuation	Mix bypass air in core
Number of lobes	18	18	18
Penetration ratio (mixer diameter / duct diameter)	0.7	0.7	0.7
Type	solid	porous	lobed centerbody
Mixing efficiency goal (Frost's Correlation, Reference 4)	85%	85%	85%
Mixer length / duct diameter	0.81	0.81	0.81

The three configurations were evaluated in RAMPANT using the same process as used for the TFE731-60 mixer nozzle evaluation. This process involved calculating the interior nozzle solution for the aerodynamic performance analysis, and a plume solution for the acoustic analysis, which used a flow profile created from the interior solution. Figure 41 shows the interior nozzle grid for Configuration 3, the most complex geometry of the three configurations.

To have a fair comparison between the various acoustic solutions core and bypass mass flows were set and model inlet total pressures were allowed to vary. This allowed the analysis to be completed at a constant bypass ratio and not allow noise to be dictated by core flow reduction.

All mixer nozzle configurations were run using identical boundary conditions set to the base TFE731-40 cycle point used for the high-power 2-D axisymmetric acoustic point. For the interior solution, the core and bypass inlet boundaries were modeled as mass flow inlet boundaries. As with the TFE731-60 model, only a half lobe was modeled, thus the sides of the model were modeled as symmetry boundaries. RAMPANT's standard k-ε model was used for all analyses. The nozzle aerodynamic model was adapted to y^+, gradients of static pressure, and gradients of total temperature. The final adapted model contained about 200 000 fluid cells.

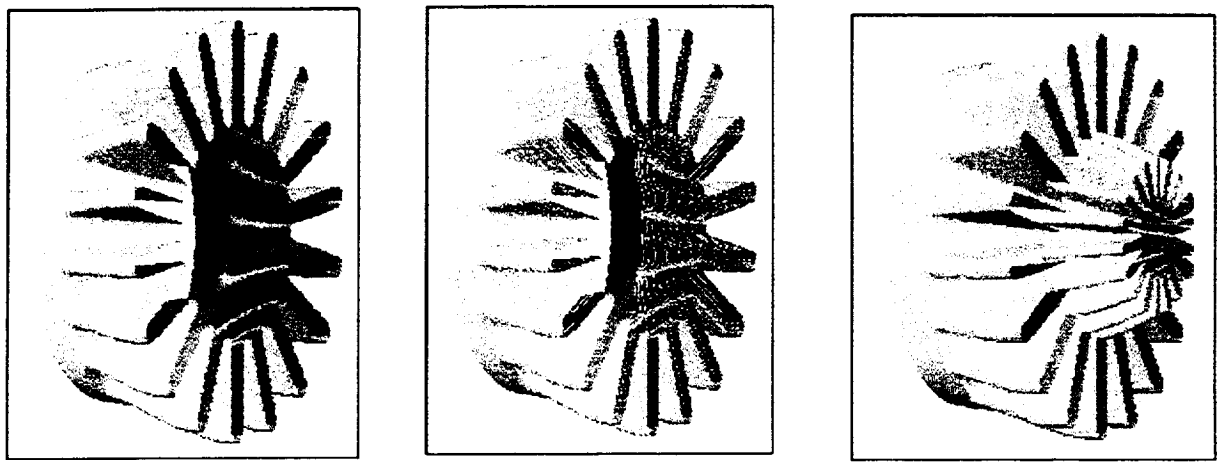

(a) Configuration 1 (b) Configuration 2 (c) Configuration 3

Figure 40. Three Innovative Mixer Design Concepts Have Been Evaluated.

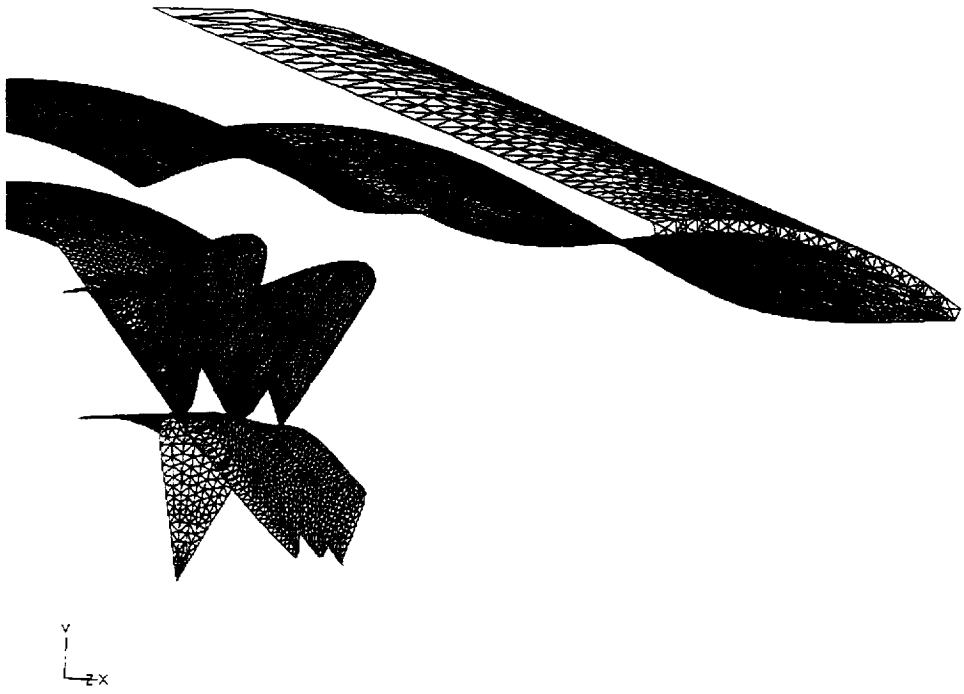

Figure 41. The Lobed Centerbody (Configuration 3) Resulted in the Most Complicated Computational Domain of the Three Configurations.

Figure 42 shows various axial cuts of total temperature for the base TFE731-40 compound nozzle, Configuration 1, Configuration 2, and Configuration 3. These contour plots show the lack of thermal mixing for the base compound nozzle and the large improvement in mixing for all of the mixer nozzle configurations. For the mixer configurations, the porous mixer (Configuration 2) mixes more effectively than the other two configurations. Additionally, the core/plug mixer concept (Configuration 3) improved cooling to nozzle centerline and shows that the core plug was over designed and brought excessive cooling air to the centerline of the engine, thus reducing mixing efficiency over Configuration 1.

Basic aerodynamic performance of the base compound mixer nozzle and the three advanced mixer configurations are shown in Table 5. The base compound nozzle had the lowest pressure losses and the core/plug mixer had the highest losses. The high pressure loss from the porous mixer is due to the pressure drop seen for flow passing through the mixer and the high pressure loss for the core/plug mixer is due to the added skin friction loss for flow passing over the additional mixer.

Table 5. Result of RAMPANT Performance Evaluation of Mixers.

RAMPANT Estimate - Takeoff Thrust Condition

Configuration	Description	Mixing Efficiency	Core Pressure Drop	Bypass Pressure Drop	Rating Station Thrust Coefficient*
	Base Compound	16.9%	0.7%	0.52%	0.981
1	18 Lobe	66.4%	1.1%	0.63%	0.987
2	Porous	67.9%	2.1%	0.61%	0.985
3	core mixer	64.8%	2.4%	0.65%	0.979

* Mixer provides significantly higher performance in cruise

(a) TFE731-40 Compound Nozzle (b) Configuration 1

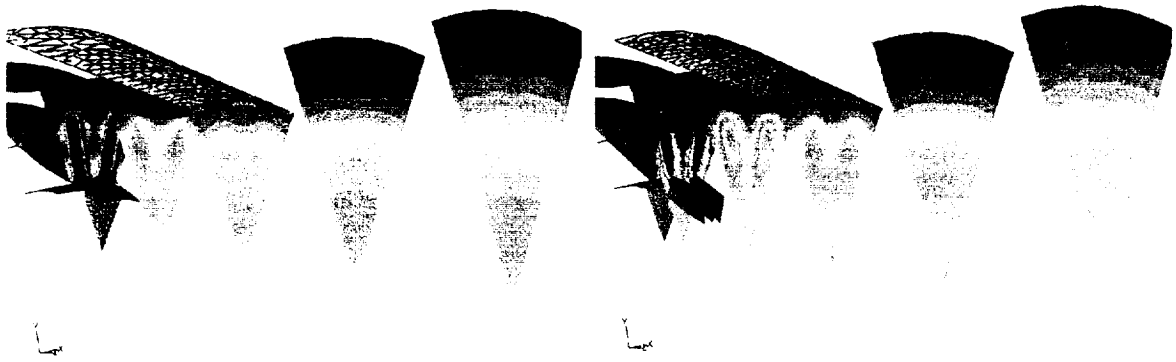

(c) Configuration 2 (d) Configuration 3

Figure 42. Total Temperature Contours Show the Relative Mixing Efficiency of the Four Nozzle Configurations.

Effect of the mixer can be seen in the RAMPANT calculated thermal mixing efficiency. The mixing efficiency varied from 16.9 percent for the base compound nozzle to 65-68 percent for the various 18-lobe mixer configurations. This is a significant improvement when compared to the 14-lobe TFE731-60 mixer that had thermal mixing efficiencies of 45 to 47 percent. However, increasing thermal mixing efficiency by increasing lobe count above 18 may not be fruitful since, as seen in Figure 42, circumferential temperature variation is minimal at the nozzle exit plane. To increase thermal mixing efficiency, the radial temperature variation needs to be reduced. This reduction can be accomplished by increasing the lobe penetration; however, increasing lobe penetration can cause cooling problems on the bypass outer shroud.

The plume was modeled using the same procedure as done for the TFE731-60 mixer model. This procedure used a flow profile generated from the interior solution as the input flow boundary to the plume solution. The mesh used for the plume evaluation contained about 75 000 fluid cells.

Figure 43 shows the contours of TKE for the base compound nozzle and the three advanced mixer configurations. The plume TKE levels for the base compound nozzle show peak levels in the plume of about 40 000 ft^2/sec^2. The other various mixer configurations have significantly lower levels of TKE, thus showing the improvements due to the mixer nozzle. All plumes appear to have the same general shape, however, Configuration 3, the core/plug mixer, has the lowest overall TKE levels even though it has the lowest mixing efficiency. The reason for this effect is not known.

For each nozzle configuration, the 3-D RAMPANT CFD flowfield data were interpolated onto a 2-D slice. The slice is a plane which cuts the 3-D wedge lengthwise between the two symmetry surfaces. Based on the assumption that the particular slice taken makes little difference in the jet noise computation for the frequency range of interest , the slice was arbitrarily taken to be at 5.63 degrees, about midway between the symmetry surfaces. Flowfield data, which are defined on an unstructured grid on this planar surface, were interpolated onto a structured mesh of about 20 000 points (169 points axially x 119 radially).

The results of the noise predictions are plotted in Figures 44 and 45, and are compared to the results from the TFE731-40 nozzle prediction All predictions were for the takeoff power condition and used the same MGB input parameter (BETAMC) values. Note that the peak power levels for Configurations 1 and 3 are around 2.5 dB below the peak power level for the TFE731-40 case. Figure 44 shows that the MGB program estimates that the advanced mixer configurations will meet the 3 dB noise reduction goal.

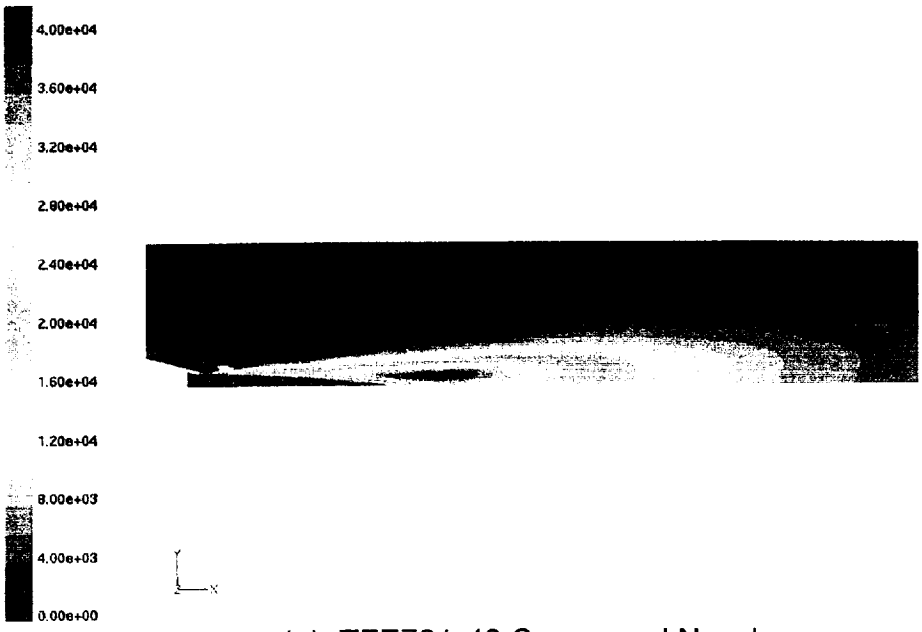

(a) TFE731-40 Compound Nozzle

(b) Configuration 1

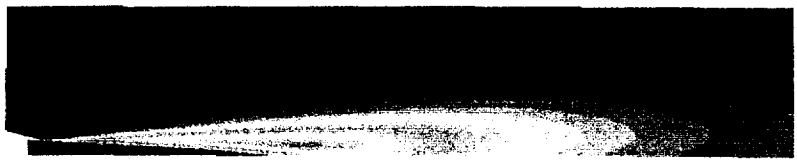

(c) Configuration 2

(d) Configuration 3

Figure 43. Contours of Turbulent Kinetic Energy Show the Effect of Mixer Design on the Jet Plume Turbulence Structure.

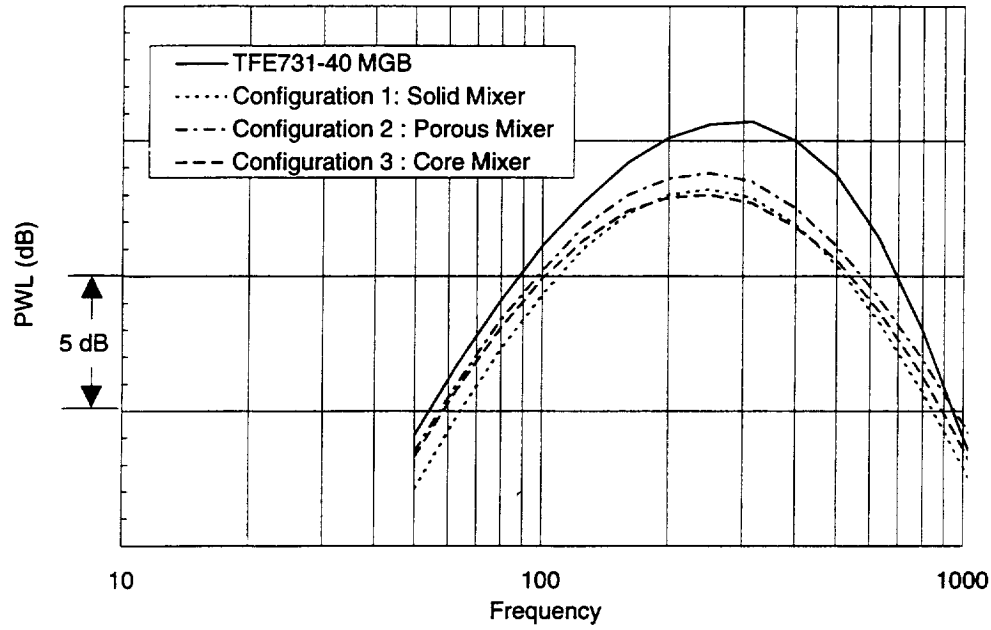

Figure 44. The MGB Predictions Show the Anticipated Acoustic Benefit of the Three Mixer Nozzle Configurations.

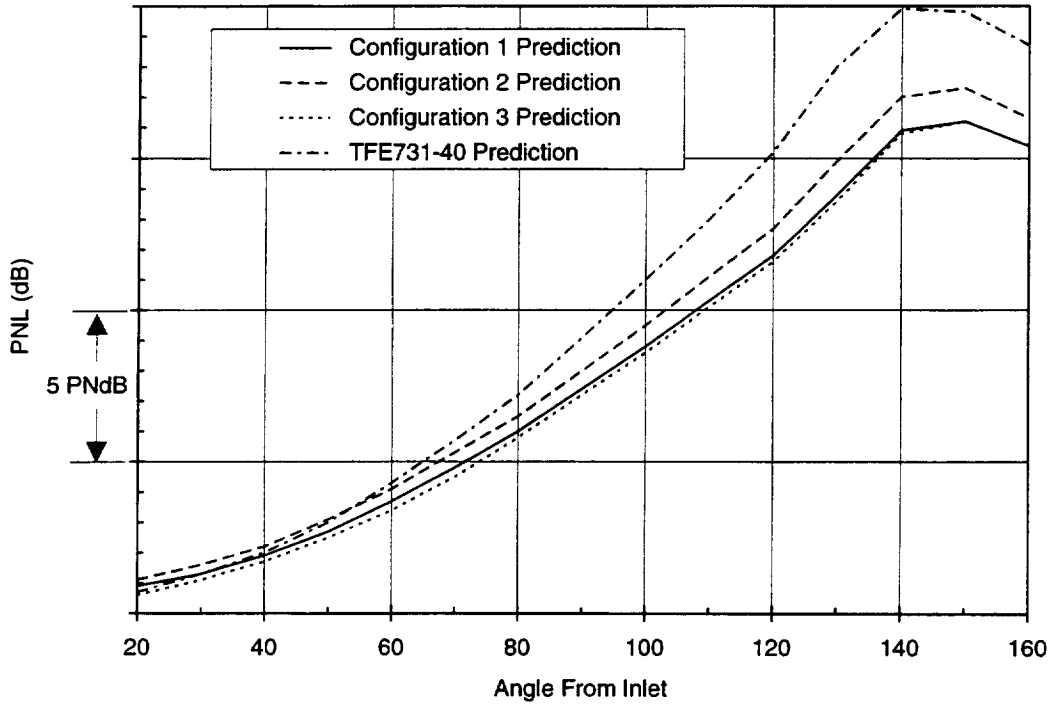

Figure 45. The MGB Program Estimates More Than a 3 dB Noise Reduction for the Advanced Mixer.

4.0 FINAL AMNS AERODYNAMIC DESIGN

A final mixer (Figure 46) was designed based on the experience gained in the analysis efforts of this task. The optimized mixer incorporated various benefits exhibited from the earlier test cases. The optimized design used a porous 18-lobe core/bypass cut-back mixer design with a cut-back lobed centerbody The penetration ratio of the core/bypass mixer was increased from 70 to 75 percent. Advantages of this concept were seen as:

- The 18-lobed design has superior circumferential mixing relative to the 14-lobed TFE731-60 mixer.

- A higher penetration mixer design increases radial mixing.

- The porous mixer improves mixing efficiency, although pressure loss increased and jet noise was higher than the other configurations. A lower open area was selected to keep mixing efficiency and lower mixer pressure drop.

- The lobed centerbody lowers jet noise, but it also increases friction losses and over-cooled the centerline of the mixer nozzle. A highly cut-back lobed centerbody design was selected which would lower friction losses, while maintaining the acoustic benefits.

The CFD solution was evaluated in the same manner as the earlier configurations by evaluating a near-field solution for nozzle performance, and plume solution for the jet noise acoustic evaluation. RAMPANT's standard k-ε model was used and the model was evaluated using a 1/2 lobe model using symmetry boundaries. The near field solution used over 200 000 fluid cells, and the plume solution used over 100 000 fluid cells.

The increased penetration ratio improved nozzle thermal mixing more than 5 percent compared to the base nozzle configurations. Figure 47 shows the contours of total temperature at several stations inside and outside of the nozzle. The core/plug mixer still appears to be slightly oversized, as demonstrated by the cooler center flow. Increasing the cutback of the core/plug mixer would further improve thermal mixing and reduce mixer friction losses. Peak TKE levels are similar to the previous mixer configurations. Table 6 summarizes the overall performance of the nozzle. The final configuration has the best mixing efficiency and rating station thrust coefficient of any of the configurations examined.

Table 6. Nozzle Performance Results for the Final Mixer Nozzle Configuration.

Conf.	Description	η_{mix}	$\Delta P/P_T$core	$\Delta P/P_T$bypass	$Cf_{rating\ station}$
Baseline	Compound	16.9%	0.7%	0.52%	0.981
1	Base line mixer	66.4%	1.1%	0.63%	0.987
2	Porous mixer	67.9%	2.1%	0.61%	0.985
3	Lobed center body	64.8%	2.4%	0.65%	0.979
Final	**Final configuration**	**72.9%**	**1.5%**	**0.56%**	**0.988**

The results of he RAMPANT flowfield calculations were formatted for acoustic calculations with the MGB code in the same manner as the previous mixers. Figure 48 shows that the final mixer configuration is predicted to have a lower overall acoustic power than any of the other mixer configurations. Figure 49 shows the estimated perceived noise level evaluation of the final mixer configuration. Note that the PNL values increased very slightly due to some higher frequency noise content in the spectrum (Figure 48). However, the acoustic differences are very small.

5. CONCLUSIONS

From the MGB code implementation, it is concluded that:

1) The MGB code has been successfully installed in the nozzle design system at AlliedSignal Engines.

2) A RAMPANT solution was successfully obtained for the Khavaran nozzle test case for the MGB program.

3) RAMPANT grid adaptation on dU/dy and Reynold's stress was necessary to correctly model the turbulent kinetic energy in the jet plume.

4) The RAMPANT CFD results agree well with the PARC results for the Khavaran nozzle test case, especially considering the differences in flow modeling between the two codes.

5) RAMPANT Journal files can easily be generated to convert results from the RAMPANT unstructured grid to the structured grid required by MGB.

6) The MGB noise analysis using RAMPANT results for the Khavaran nozzle test case adequately matched the MGB results using the PARC CFD analysis.

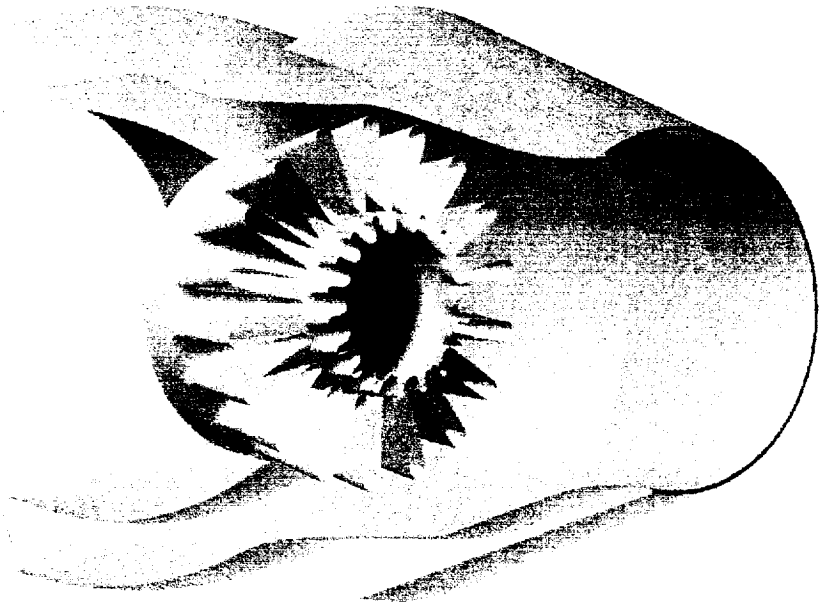

Figure 46. The Optimized Mixer Design Incorporates the Best Concepts of the Three Previous Mixer Designs.

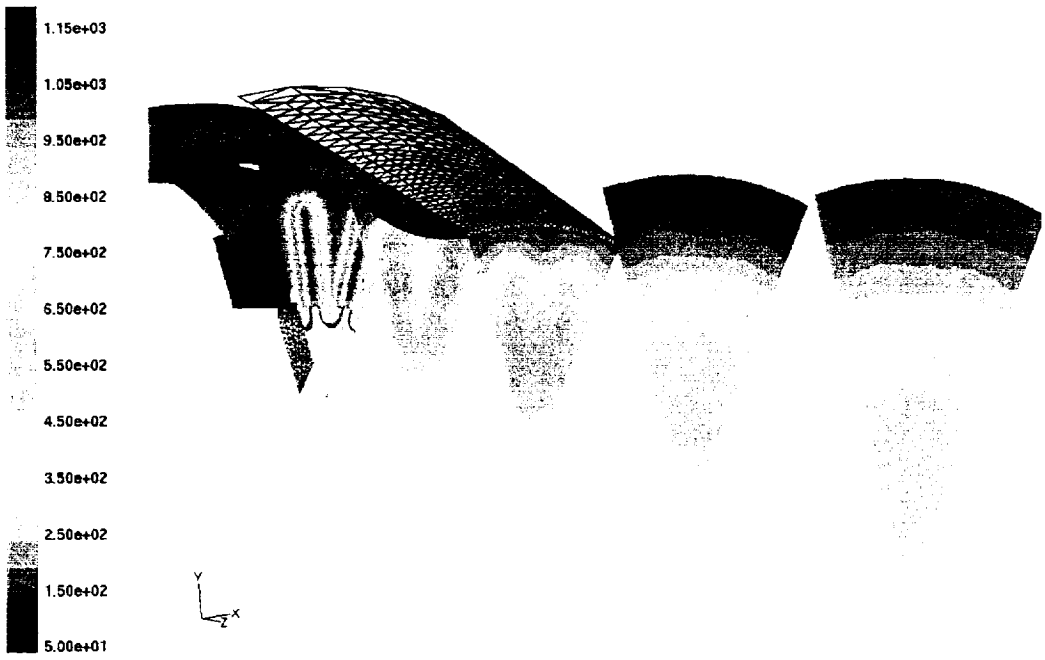

Figure 47. Optimized Mixer Shows Improved Thermal Mixing Efficiency Relative to the Three Initial Configurations.

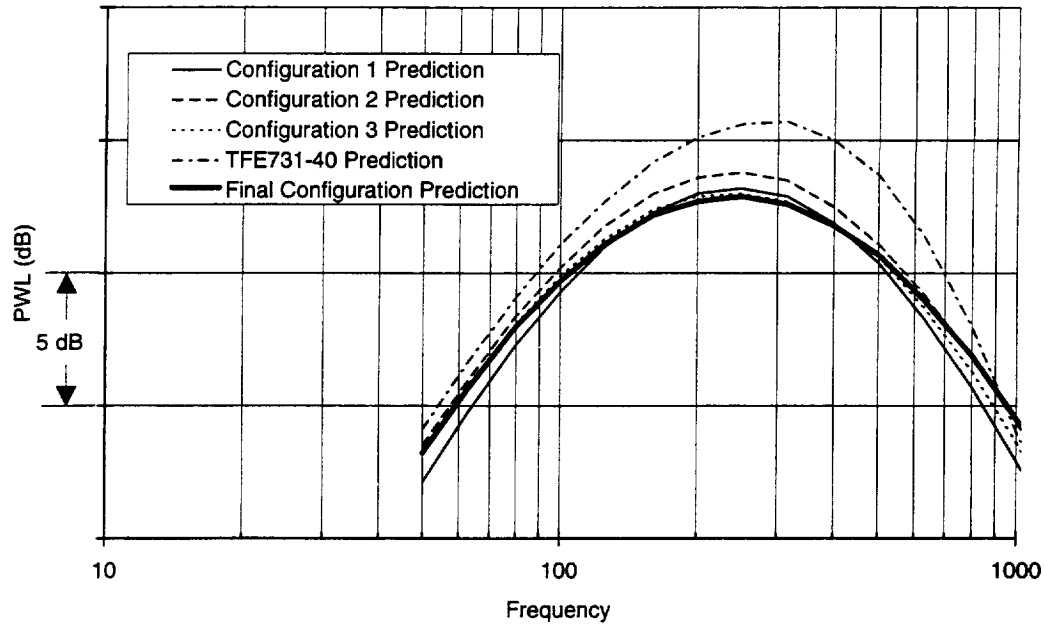

Figure 48. The MGB Predictions Show the Anticipated Acoustic Benefit of the Final Mixer Nozzle Configuration.

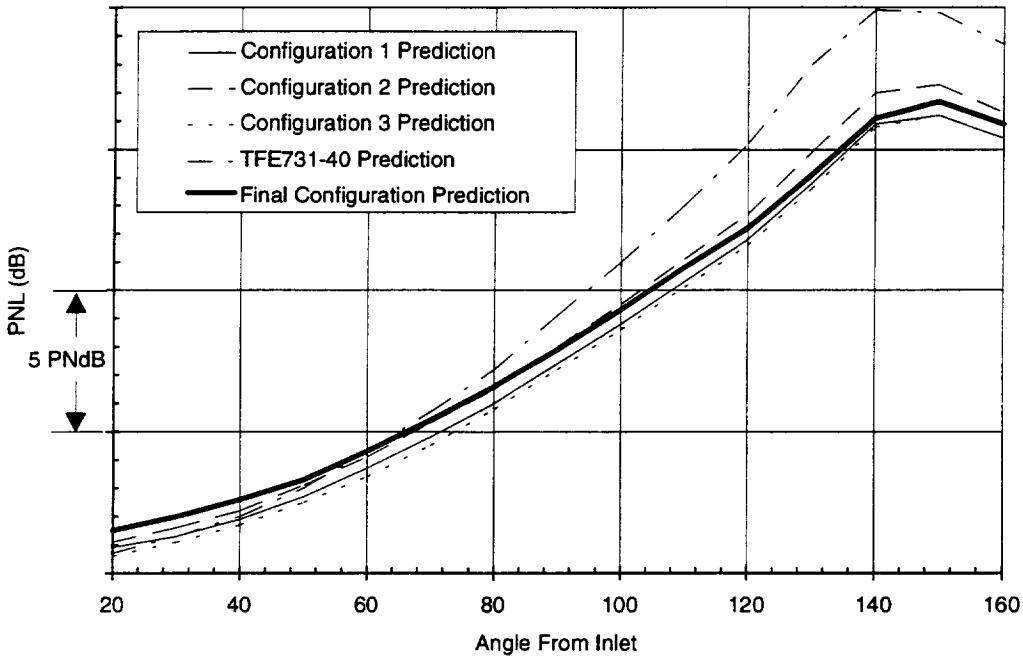

Figure 49. The MGB Program Estimates More Than a 3 dB Noise Reduction for the Advanced Mixer.

From the validation of the RAMPANT/MGB noise predictions for the unmixed TFE731-40 nozzle system, it is concluded that:

1) RAMPANT produced a successful aerodynamic solution for the TFE731-40 compound nozzle operating statically, simulating an engine operating on a test stand.

2) Analysis of the RAMPANT CFD results of the TFE731-40 with the MGB program produced predicted sound power levels that agree quite well with the measured data from full-scale static engine tests.

3) Comparison of sound pressure levels predicted by RAMPANT/MGB and measured on the TFE731-40 engine show good agreement near the jet axis, but the noise levels are overpredicted at angles closer to the inlet.

4) A value of BETAMC=0.2 was required to achieve the satisfactory agreement of prediction with data.

From the validation of the RAMPANT/MGB noise predictions for the TFE731-60 (TFE731-5A) nozzle system, it is concluded that:

1) A successful RAMPANT analysis of the TFE731-60 flowfield was successfully obtained by performing a detailed interior flow aerodynamic flow solution which was then coupled to a three dimensional plume solution.

2) The RAMPANT program accurately predicted the nozzle thrust coefficient as measured in a rig test. Nozzle flow was slightly underpredicted.

3) A procedure was developed to interpolate the 3-D RAMPANT solution onto the 2-D axisymmetric MGB computational grid. Variation in circumferential position of the 2-D slice had minimal effect on the computed noise.

4) The predicted sound power level for the TFE731-60 did not agree as well with measured static engine data as the TFE731-40. Although a reduction in the predicted noise level due to the mixed flow was observed, the reduction was not as significant as the measured data.

The analysis of the V2 mixer from the E^3 study showed that:

1) The V2 mixer can be successfully modeled using the unstructured grid procedures of RAMPANT.

2) Peak temperatures predicted by RAMPANT in the mixer exit flowfield were within 5 percent of the values measured by the exit probes.

3) The circular pattern of total pressure for the mixer lobes predicted by RAMPANT did not match the crescent shape patterns measured by the total pressure rakes.

4) RAMPANT predictions of the axial velocities generally agreed well with the velocities measured with the LDV system.

5) The RAMPANT/MGB predictions of the V2 mixer nozzle noise tended to be 3-5 dB higher in peak noise level than the measurements. In addition, the maximum frequency of the noise was also overpredicted.

The analysis of the 3 candidate mixer nozzle configurations showed that:

1) All three configurations showed improved nozzle performance as compared to the baseline TFE731-40.

2) Configuration 1, the advanced hardwall mixer, provided the best overall nozzle efficiency.

3) The porosity of Configuration 2 improved mixing efficiency, but introduced a 1 percent increase in the core pressure drop.

4) The lobed centerbody of Configuration 3 more effectively transferred cool bypass air to the nozzle centerline, and resulted in the lowest TKE values in the plume.

5) Configuration 3 produced the lowest noise levels of the three configurations.

Based on the results of the analysis of the 3 advanced mixer configuration a final configuration was defined with the following features:

- 5% porosity
- 18 lobes
- core/bypass cut-back mixer design
- cut-back lobed centerbody
- 75% penetration ratio of the core/bypass mixer

This final configuration resulted in a thermal mixing efficiency that was 5 percent higher than all of the original advanced designs based on the RAMPANT calculations. The results of the MGB noise calculations show that the final design will exceed the design goal of a 3 dB reduction in noise as compared to the baseline TFE731-40.

6.0 REFERENCES

1. Khavaran, A., Krejsa, E. and Kim, C., "Computation of Supersonic Jet Mixing Noise for an Axisymmetric Convergent-Divergent Nozzle," Journal of Aircraft, Vol. 31, No. 3., 1994, pp. 600-608.

2. Measurement of Far Field Noise from Gas Turbine Engines During Static Operations, Society of Automotive Engineers Aerospace Recommended Practice 1846, February 1990.

3. Shin, H-W. and Babbitt, B., "Experimental Study of Exhaust System Mixers for a Subsonic Jet Noise Reduction," AIAA Paper 96-2650, July, 1996.

4. Frost, T., "Practical Bypass Mixing Systems for Fan Jet Aero Engines," The Aeronautical Quarterly, May 1966.

REPORT DOCUMENTATION PAGE

Form Approved
OMB No. 0704-0188

1. AGENCY USE ONLY (*Leave blank*)	2. REPORT DATE	3. REPORT TYPE AND DATES COVERED
	September 1999	Final Contractor Report

4. TITLE AND SUBTITLE

Forced Mixer Nozzle Optimization

5. FUNDING NUMBERS

WU–538–03–11–00
NAS3–27483, Task Order 7

6. AUTHOR(S)

Yogi Sheoran, Robert Hoover, William Schuster, Morris Anderson and Donald S. Weir

7. PERFORMING ORGANIZATION NAME(S) AND ADDRESS(ES)

AlliedSignal Engines
P.O. Box 52181
Phoenix, Arizona 85072–7181

8. PERFORMING ORGANIZATION REPORT NUMBER

E–11723

9. SPONSORING/MONITORING AGENCY NAME(S) AND ADDRESS(ES)

National Aeronautics and Space Administration
John H. Glenn Research Center at Lewis Field
Cleveland, Ohio 44135–3191

10. SPONSORING/MONITORING AGENCY REPORT NUMBER

NASA CR—1999-209160

11. SUPPLEMENTARY NOTES

Project Manager, Naseem U. Saiyed, Structures and Acoustics Division, NASA Glenn Research Center, organization code 5940, (216) 433–6736.

12a. DISTRIBUTION/AVAILABILITY STATEMENT

Unclassified - Unlimited
Subject Categories: 07, 71, and 34 Distribution: Nonstandard

This publication is available from the NASA Center for AeroSpace Information, (301) 621–0390.

12b. DISTRIBUTION CODE

13. ABSTRACT ***(Maximum 200 words)***

Computational fluid dynamic (CFD) and computational acoustic analyses (CAA) were performed for a TFE731-40 compound nozzle, a TFE731-60 mixer nozzle and an Energy Efficient Engine (E^3) mixer nozzle for comparison with available data. The CFD analyses were performed with a three dimensional, Navier-Stokes solution of the flowfield on an unstructured grid using the RAMPANT program. The CAA analyses were performed with the NASA Glenn MGB program using a structured grid. A successful aerodynamic solution for the TFE731-40 compound nozzle operating statically was obtained, simulating an engine operating on a test stand. Analysis of the CFD results of the TFE731-40 with the MGB program produced predicted sound power levels that agree quite well with the measured data from full-scale static engine tests. Comparison of the predicted sound pressure with the data show good agreement near the jet axis, but the noise levels are overpredicted at angles closer to the inlet. The predicted sound power level for the TFE731-60 did not agree as well with measured static engine data as the TFE731-40. Although a reduction in the predicted noise level due to the mixed flow was observed, the reduction was not as significant as the measured data. The analysis of the V2 mixer from the E^3 study showed that peak temperatures predicted in the mixer exit flowfield were within 5 percent of the values measured by the exit probes. The noise predictions of the V2 mixer nozzle tended to be 3-5 dB higher in peak noise level than the measurements. In addition, the maximum frequency of the noise was also overpredicted. An analysis of the 3 candidate mixer nozzle configurations demonstrated the feasibility of using centerbody lobes and porosity to improve mixing efficiency. A final configuration was designed with a predicted thermal mixing efficiency that was 5 percent higher than the 3 candidate mixers. The results of the MGB noise calculations show that the final design will exceed the design goal of a 3 dB reduction in noise as compared to the baseline TFE731-40.

14. SUBJECT TERMS

Subsonic; Acoustics; Mixers; MGB; CAA; Jet engines; Jet noise; Forced mixers

15. NUMBER OF PAGES
61

16. PRICE CODE
A04

17. SECURITY CLASSIFICATION OF REPORT	18. SECURITY CLASSIFICATION OF THIS PAGE	19. SECURITY CLASSIFICATION OF ABSTRACT	20. LIMITATION OF ABSTRACT
Unclassified	Unclassified	Unclassified	